

**The variability of currents in the Yucatan Strait:
Analysis of results from a numerical ocean model**

Tal Ezer^{*}, Lie-Yauw Oey^{*}, Wilton Sturges⁺ and Hyun-Chul Lee^{*}

^{*} Program in Atmospheric and Oceanic Sciences
P.O.Box CN710, Sayre Hall, Princeton University,
Princeton, NJ 08544-0710

⁺ Department of Oceanography
Florida State University
Tallahassee, FL 08360

May, 2002

ABSTRACT

Despite the importance of flow through the Yucatan Strait as a major component of the subtropical gyre that feeds the Gulf Stream, and recent additional observations, little is known about the forcing and physical parameters that relate to the current structures in the Strait. This paper attempts to improve our understanding of the flow through the Strait with a detailed analysis of the currents extracted from a five-year, primitive-equation model of the circulation in the Gulf of Mexico and the Caribbean Sea. The analysis is in two parts: firstly, a comparison with observations of the overall statistics – the Loop Current (LC) variability and periods of Loop Current Eddy (LCE) shedding, as well as the means and standard deviations (SD) of transports and currents, and secondly an Empirical Orthogonal Function (EOF) and coherency analysis that attempts to identify the forcing and physical parameters responsible for the dominant modal fluctuations in the Strait.

The model LC sheds seven LCEs in four years (allowing one-year spin-up) at irregular time intervals (6.6, 7.1, 5.3, 11.9, 4.2, 10.9) months. The model's upper (thickness $\sim 800\text{m}$) inflow into the Gulf of Mexico occupies two-thirds of the Strait on the western side, with a near-surface maximum (4-year) mean of around 1.5 m s^{-1} and $\text{SD} \approx 0.4 \text{ m s}^{-1}$. Three (return) outflow regions are identified, one in the upper layer (thickness $\sim 600\text{m}$) on the eastern third of the strait, with mean near the surface of about 0.2 m s^{-1} and $\text{SD} \approx 0.14 \text{ m s}^{-1}$, and two deep outflow cores, along the western and eastern slopes of the strait, with (Mean, SD) $\approx (0.17, 0.05)$ and $(0.09, 0.07) \text{ m s}^{-1}$, respectively. These flow structures, and values of the means and variances, as well as the range of variations in the modeled Strait transport, from 16 to 34 Sv ($1 \text{ Sverdrup} = 10^6 \text{ m}^3 \text{ s}^{-1}$), agree quite well with observations by Maul et al. (1985), Ochoa et al. (2001), and Sheinbaum et al. (2002). The deep return transport below 800 m was found to correlate with changes in the Loop Current extension area, in agreement with the observational analysis by Bunge et al. (2001).

The EOF mode#1 of the along-strait currents contains 50% of the total energy. It is surface-trapped, is 180° out of phase across the channel, and correlates well (correlation coefficient $\gamma \approx 0.8$) with the cross-channel vacillations of the LC frontal position. Its time-series at times visually correlates also with the inflow transport and LCE-shedding events but the correlation is not statistically significant. The EOF mode#2 contains 18% of the energy, and its structure mimics that of the mean: dominated by two vertically more coherent regions that are 180° out of phase across the Strait. The mode is dominated by two periods, approximately 11 months and 2 months respectively, and correlates ($\gamma \approx 0.7$) with the inflow transport. The third and fourth modes together account for 18% of the total energy. Their combined time-series correlates ($\gamma \approx 0.66$) with the deep current over the sill, and is dominated by fluctuations with a period ≈ 205 days coincident with the dominant low-frequency fluctuations inherent in Maul et al.'s (1985) sill measurement. It is concluded that the dominant mode of flow fluctuations in the Yucatan Strait is caused by LC cross-frontal movements not directly related to LCE-sheddings, while higher modes correspond to transport fluctuations that affect sheddings, and to a bottom-trapped current fluctuations, the cause of which has yet to be uncovered.

1. Introduction

The Yucatan Strait (YS) connects the Caribbean Sea with the Gulf of Mexico (GOM). As part of the North Atlantic circulation, flow from the subtropical gyre enters the Caribbean Sea and into the Gulf of Mexico, to form the Loop Current (LC), which then exits through the Florida Straits (FS) (Fig. 1). Except for the relatively small water mass exchange through river runoffs and surface buoyancy fluxes, the transport in and out of the GOM, about 28 Sv (1 Sverdrup = $10^6 \text{ m}^3 \text{ s}^{-1}$) (Schmitz and Richardson, 1991; Schmitz and McCartney, 1993; Johns et al., 2002), is controlled by inflow through the YS and outflow through the FS. While the sill depth at the YS is about 2000 m depth, the FS is much shallower at about 800 m. Therefore, it has been suggested (e.g., Maul, 1977) that if there exists a deep transport in the YS below the sill depth of the FS, it must be balanced by excess inflow transport in the upper layers that accounts for variations in the volume of the LC as it extends and shed eddies into the GOM. This would imply that variations in the deep layers are correlated with variations in the LC. However, attempts by Maul et al. (1985) to find a relation between the LC and the deep flow in the YS, were unsuccessful. Despite the potential importance of the YS transport as the principal driver of the LC, its likely relation to the LCE-shedding process, and as the major flow conduit that feeds the mighty Gulf Stream, it is surprising that since Maul's study, almost two decades elapsed before the extensive measurements of Bunge et al. (2001), Ochoa et al. (2001), and Sheinbaum et al. (2002) in the Strait. These recent observations cast new light into the detailed velocity structures in the Strait, and explain why the early observations by Maul over the sill did not show the expected correlation of flow with the LC. Specifically, the new observations show that most of the return deep flow is found along the eastern and western slopes of the YS and not in the middle of the sill as was previously thought. Moreover, the deep transports from the new observations do agree

with the hypothesis set forth by Maul and are correlated with the variations in the LC (Bunge et al. (2001).

Perhaps in part due to the lack of observations prior to the more recent ones cited above, models of the Gulf tend to avoid direct reference to the dynamics of the YS (e.g. Sturges et al., 1993; Welsh and Inoue, 2000). This is understandable for early models, as for example in the pioneering work of Hurlburt and Thompson (1980), in which the prime objective was to gain a deeper understanding of the processes of LCE-shedding, propagation and decay inside the Gulf. Indeed, Hurlburt and Thompson's explicit specifications of transport at YS preclude a direct dynamical study of the free interaction that must exist between the LC in the Gulf and the Yucatan inflow from the Caribbean Sea. On the other hand, even in this simplified model setting, Hurlburt and Thompson's study was able to demonstrate the sensitivity of the LCE-shedding process to details of the YS-inflow profile they specified. In part inspired by Hurlburt and Thompson's work, Oey (1996) emphasized the importance of the interaction between the Gulf and the Caribbean Sea, and found significant outflow (fluctuations) in the deep layers in YS that correlate with inflow near the surface, as well as with episodes of LCE-shedding. However, Oey's work stops short of clarifying the details of these relations, the spatial and temporal structures of the velocity profiles across the Strait, as well as the natures of the forcing that produce the fluctuations.

In this paper, we study in more details the spatial and temporal structures of flow across the Yucatan Strait, using a model that has double the grid resolution of that used by Oey (1996; 5-10km versus 20km), and an expanded domain that includes the entire Caribbean Sea (instead of the northwestern portion of it), as well as the Gulf. The finer grid now results in a maximum four-year mean inflow speed of about 1.5 m/s (see below) at the Strait, a value that is more consistent with that observed (Ochoa et al., 2001; Sheinbaum et al., 2002). The expanded domain eliminates any ambiguity that might result in the interpretations of Straits dynamics because of uncertainty in the upstream

boundary conditions in a more limited Caribbean Sea domain. Our primary objectives are to describe flow structures across the Strait, and to relate them to LC variability and LCE-shedding events. On a more limited basis, we will also attempt to relate the model results to observations.

The paper is organized as follows: First, the numerical model is briefly described in section 2, then the model results are described in sections 3, and finally, a summary and conclusions are offered in section 4.

2. The Numerical Model

The results we analyze in this paper are based on one of the experiments to be described in more details in Oey et al. (2002). The model is based on the Princeton Ocean Model (POM, Blumberg and Mellor, 1987; Mellor, 1996). The model domain extends westward from 55°W and also north of 5°N , thus including the Gulf Stream, the Gulf of Mexico and the Caribbean Sea. Inflow and outflow transports are specified across 55°W . These transports determine the depth-integrated velocities at the boundary, and are meant to account for the large-scale transports (Svedrup + thermohaline) through 55°W . The three-dimensional velocity, temperature and salinity fields at the open boundary are calculated according to Oey and Chen (1992). For example, the temperature and salinity fields are advected using one-sided difference scheme when flows are eastward (that is, outflow), and are prescribed from the GDEM monthly temperature and salinity climatology (Teague et al., 1990) when flows are westward. These open-boundary specifications also set the baroclinic structure, which in the present case is largely geostrophic through the thermal-wind balance. The prescribed open boundaries are sufficiently removed from the Gulf of Mexico that there is a free dynamical interaction between the Caribbean Sea and the Gulf through the Yucatan Strait (Oey, 1996). Horizontal resolution of the curvilinear orthogonal grid ranges from about 10 km in the

vicinity of the YS to about 5 km on the northern continental shelf. There are 25 vertical sigma levels, with higher resolution near the surface and near the bottom, so that wind-driven and bottom-trapped topographic Rossby waves (Oey and Lee, 2002) can be better resolved. Surface forcing includes wind stress in 6-hour intervals obtained from the European Center for Medium range Weather Forecast (ECMWF) and surface heat flux and buoyancy forcing based on monthly climatology. Though the full model can incorporate data assimilation that use satellite-derived sea surface temperature and altimeter data (Ezer et al., 2002; Wang et al., 2002); this study only analyzes the wind-driven model without the assimilation, and focus on four years simulations (1993 through 1996), following a one year spin up period. This allows us to study the natural variability of the model dynamics. One should keep in mind, however, that in regions with intense meso-scale activity such as in the Gulf of Mexico, the time-evolution of a model without data assimilation does not generally correspond to that observed.

3. Model Results

3.a. The Yucatan Strait velocity, transport, and variations in the Loop Current extension

Until recently, our knowledge of the deep flow in the Yucatan Strait was largely based on the 1977-1980 current-meter observations just above the sill at 1895 m reported by Maul et al. (1985) (see also Burkov et al., 1982). While we cannot directly compare the model result with Maul et al.'s measurements (because of different time-periods and lack of data assimilation in the simulations analyzed here), it is useful to compare the means and standard deviations (SD) over a three-year period as in the observed record (Figure 2). The figure shows that both model and observation give a southwestward mean flow, though the model's southward flow is more intense. Of interest is that the model has attained the observed level of variability especially in the along-channel component

(SD $\approx 0.04 \text{ m s}^{-1}$ in both model and observation). The modeled cross-channel SD is 30% less than observed, which indicates that the modeled currents are more constrained by bottom topography. Spectral analysis of the v component of the flow from the observations and from the model (Fig. 3) reveals that both records have high frequency oscillations, as well as longer-term fluctuations. On the low-frequency portion, of particular interest is the occurrence of 205-day peak in both the model and observed records. We will later show that this corresponds to higher modal fluctuations in the currents. There is also a 341-day peak in the model's spectra; this we will show to correspond to the low-frequency modulation of the transport time series. We do not know why this peak (or a longer period mode) is not present in the observed record. For periods ≈ 114 days and shorter, both spectra show peaks at 114, 93, 64, 37 day and shorter. Except for the 114-day peak, observation is more energetic at the higher-frequency end: 37, 32 and 18-day. There is some evidence in the model that the shorter-period (<114 days) fluctuations are topographic Rossby waves, in that the steep bottom slope and value of stratification support such waves with periods as short as 10 days, and that energy intensify near the bottom (not shown; c.f. Oey and Lee, 2002), though clearly a detailed study preferably in conjunction with observations is necessary to confirm the existence of these waves.

The spatial structure of the mean and standard deviation of the along channel (v -component) flow are shown in Fig. 4. The section is near 21.95°N , slightly on the north side of the sill (Fig. 1). The model has 20 horizontal grid points across the Strait (grid size ≈ 10 km). The mean flow is characterized by several cores of local maxima in flow speed. The core of the inflow into the GOM is at 3 m depth on the western side of the strait and has a maximum mean flow of 1.48 m s^{-1} and SD of 0.23 m s^{-1} . An outflow core on the eastern side of the strait at ~ 30 m depth has maximum mean flow of -0.25 m s^{-1} and SD of 0.14 m s^{-1} . This return flow is more extended and stronger (by about a factor of two) in the model than it is in the observations (Ochoa et al., 2001; Sheinbaum et al.,

2002). The core of the deep outflow on the western side of the strait at 1300 m depth has mean flow of -0.17 m s^{-1} and SD of 0.05 m s^{-1} , in good agreement with the observed undercurrent deep flow of about 0.2 m s^{-1} (Ochoa et al., 2001). The core of the outflow on the eastern side of the strait at 1400 m depth has mean flow of -0.09 m s^{-1} and SD of 0.07 m s^{-1} . Another deep core has a northward velocity (inflow), and is located about 150 m above the center of the sill (the maximum of this core is 0.09 m s^{-1} , less than the first positive contour, so it is not clearly indicated in Fig. 3a). The latter flow at the center of the sill seems to contrast with the deep flow in Fig. 2 which is southwestward. The flow shown in Fig. 2, however, is at a location (Maul's current meter) about 25 km south west of the section shown in Fig. 4 (see Fig. 1); the spatial structure of the near-bottom flow, discussed later, will explain the abrupt change in bottom flow direction. The highest variability of the flow is at the edge of the inflow, near the Yucatan shelf (Fig. 4b), and is associated with temporary east-west shift in the inflow core, as will be shown in more detail later. The variability of the deep flow is of similar magnitude as the mean flow.

The variations in the flow and their relation to changes in the LC, during a three-month period (October, 1995 to January, 1996) when an eddy was shed, are demonstrated in Fig. 5. While the LC is growing, the return flow near the eastern side and on the deep slopes intensifies and occupies a growing portion of the Strait (Fig. 5a-5c). But as the eddy shedding develops, the inflow core moves offshore (eastward), which causes a reduction in the return flow on the east side and an increase in the return flow on the western slope of the strait. There are similarities between this particular period and other eddy shedding events but also some differences. Not every eddy shedding event is accompanied by offshore shift in the inflow. In any case, this example demonstrates the complicated nature of the variability of the flow in the Yucatan Strait, and the fact that the position and strength of the deep return flows vary with changes of the upper inflow core. We further look at the flow field near the surface and near the bottom (Fig. 6 and Fig. 7) during two distinct states, corresponding to Fig. 5c and Fig. 5e, respectively.

Though only 40 days separate between the two periods, the surface and bottom flow fields are completely different. During the first period, just before the eddy was separated from the LC, the surface inflow hugs the western side of the YS and then splits into a portion that follows the LC and portion that recirculates and forms the return flow on the eastern side of the YS (Fig. 6a). After the eddy was separated, the inflow core moves offshore to the center of the strait, and the southward recirculation occurs only south of the sill (Fig. 7a), thus no apparent eastern outflow is seen in Fig. 5e. The deep flow on the western slope is mostly northward during the first period (Fig. 6b), but is reversed to form a southward return flow during the second period (Fig. 7b). Note however, that large part of the deep southward flow in Fig. 7b turns northeastward near the center of the sill and recirculates back into the GOM; the other part of this deep jet continues southward along the southern slope of the sill. The location of the Maul's current meter in the center of the sill is very close to the point where the deep flow turns and thus does not represent the core of the deep outflow. This recirculation pattern of the deep flow near the center of the sill explains the discrepancy in flow direction between Fig. 2 and Fig. 4.

The variations in the YS flow and in the LC extension in the model are summarized in Fig. 8. Fig. 8a shows time series of variations of the LC extension, defined here as the area averaged sea surface elevation over the $6^\circ \times 6^\circ$ region shown in Fig. 1. The approximated time of eddy shedding events is also shown. Following the discovery of the spatial structure of the flow as shown in Fig. 4, the transport through the YS are divided into three parts: total inflow transport into the GOM, most of it above 800 m along the western side, total outflow transport above 800 m (mostly along the eastern side), and total transport below 800 m (which gives a net outflow and includes the boundary currents along the two slopes). Fig. 8b shows the transport of the inflow core and the (total) net transport across the YC, while Fig. 8c shows the outflow transport above and below 800 m. Near the time of eddy shedding events, there is often larger upper channel inflow and larger outflow. As in previous model simulations at lower

resolution and a smaller domain (Oey, 1996, Fig. 6a), there is an anti-correlation between the transport in the upper layers and the transport in the lower layers, thus suggesting that the flow is controlled by local dynamics. Analysis of observations shows similar pattern (Sheinbaum et al., 2002). Unlike the transport of the Florida Current, which is dominated by the annual cycle, with a range of about 4-5 Sv (Baringer and Larsen, 2001), in the Yucatan Strait the annual cycle is not apparent and the variability is dominated by LC extension and eddy shedding events. The total transport across the strait in the model is 25.3 Sv, with SD of 3.2 Sv and a range between 16 to 34 Sv; these values are in good agreement with recent observed estimates of a mean transport of 25 Sv and a range between 20 to 31 Sv (Ochoa et al., 2001). However, previous studies cited a larger mean transport of 28-30 Sv (Schmitz and Richardson, 1991; Schmitz and McCartney, 1993; Johns et al., 2002). This discrepancy between different estimates can be partly explained by the large range in the net transport (Fig. 8b) and the large interannual variability, which implies that a very long multi-year observed records are needed in order to accurately estimate the mean transport. The return southward flow in the model includes the upper mean transport and SD of -5.5 ± 2.5 Sv, and the bottom mean transport and SD of -2.5 ± 1.3 Sv, for a total return flow of 8 Sv. Fortuitously perhaps, the observed estimate of Ochoa et al. (2001) is also of 8 Sv total return transport. The inflow model transport of 33.4 ± 3.3 is also in good agreement with the observed estimate of 33 Sv (Ochoa et al., 2001).

Following the hypothesis (Maul et al., 1985; Bunge et al., 2001) that the deep return flow (solid line in Fig. 8c) is related to changes in the LC extension (Fig. 8a) we note that periods with relatively more deep return flow (e.g., 1996.2-1996.5) are often followed by increase in the LC extension, and these events occur usually, but not always, before or during eddy shedding events. Some large changes in LC extension, especially those with a long term nature, do not seem to relate to changes in the deep flow. Therefore, linear regression indicates small correlations between the deep flow and the

LC extension in Fig. 8. If the deep transport is related to the LC extension, as previously suggested, it may not be a direct relation but a relation between the transport and *changes* in the LC extension, since growing or receding LC is balanced by additional inflow and outflow transports, such a relation has been found in observations (Bunge et al., 2001). Therefore, as an indicator for the change in the LC extension we define here the derivative of the area averaged elevation, $\partial\langle\eta\rangle/\partial t$, and express it in cm sea level change per day. Fig. 9 shows $\partial\langle\eta\rangle/\partial t$ together with the deep transport of Fig. 8c. Since the derivatives are noisy, both the sea level change and the deep transport records have been smoothed with a 30-day low pass filter. While the correlation coefficient between the deep transport and the LC extension was less than 0.1, the correlation coefficient has increased to 0.4 (99% confidence level) for the relation with LC *changes*. Thus for most peaks in $\partial\langle\eta\rangle/\partial t$ (i.e., indicating growing LC) there are counterpart peaks in the return transport. Therefore, Fig. 9 corroborates the hypothesis of Maul et al. (1985) and the observations of Bunge et al., (2001) and Sheinbaum et al. (2002).

3.b. *Empirical Orthogonal Function (EOF) analysis of the Yucatan Strait flow field*

To get a better understanding of the spatial structure and temporal variability of the flow, Empirical Orthogonal Functions (EOF) analysis (e.g., see Bretherton et al., 1992) is conducted for the along channel (south-north) velocity field. The spatial structures of the first 4 EOF modes are shown in Fig. 10, the temporal evolutions of those modes are shown in Fig. 11, and the power spectra of the modes are shown in Fig. 12. The first mode (which contains 50% of the variability) has the characteristic of a trapped near-surface (300-400 m) western boundary current which is out of phase with the flow to the east. The temporal evolution (Fig. 11a) shows episodic events which occur about five times in four years. One example of such an event in late 1995 and early 1996 coincides with an offshore shift in the position of the inflow and the shedding of an eddy,

as shown in Fig. 5. The relation of the other episodes to eddy shedding events is not always clear (more discussion on this issue will come later). The most energetic peak in mode 1 is at 171 days (Fig. 12a). The second EOF mode (which contains about 18% of the variability) is more vertically coherent (extends to ~1000 m) and is similar in its spatial structure to the mean flow (Fig. 4a). Its time evolution (Fig. 11b) shows mostly high frequency variations on top of a long-term signal. The most energetic peak of mode 2 is at 341 days. The third and fourth EOF modes (which contain about 10% and 7% of the variability, respectively) involve a node at the center deep part of the YS, which is out of phase with flows on the eastern and western slopes. This spatial pattern can also be seen in the variations of the deep recirculation pattern shown in Figures 5-7. Note that, the spatial structure and the time evolution of modes 3 and 4 are in opposite phase with respect to each other. Note also, that, mode 4 is the only mode with significant variability near the bottom at the center of the sill. The most energetic peaks of modes 3 and 4 are at 256 and 171 days, respectively.

The most energetic peaks in the EOF modes are at periods of 171 days (5.6 months, mode 1 and mode 4), 256 days (8.4 months, mode 1 and mode 3) and 341 days (11.2 months, mode 2 and mode 4). During the four-year period analyzed here, seven LC eddies were shed at irregular time intervals (see Fig. 8a) of 6.6, 7.1, 5.3, 11.9, 4.2 and 10.9 months, thus suggesting that there may be some relation between the EOF modes and eddy shedding events. The irregular eddy shedding intervals and their periods are in general agreement with observations (Sturges, 1993; Sturges and Leben, 2000); the observations show dominant eddy shedding frequency of 6, 9 and 11 months. However, Sturges and Leben's analysis was based on 27 years of data, from 1973 to 1999, while the model analysis is based on only a four-year simulation; a more quantitative comparison with much longer simulation period is left for future studies.

We now further investigate the nature of the EOF modes, describe above, in order to identify how each mode relates to the modeled flow parameters in the YS.

EOF Mode 1- “the meander mode”. The spatial structure of the first mode, with maximum variability near the edges of the surface inflow, suggests to us that the first mode may be related to fluctuations in the upper flow position. A time series representing the east-west variations in the position of the inflow is obtained from the location of the 40 cm s^{-1} contour at sigma level 6 (i.e., the eastern edge of the inflow in Fig. 4a, which is close to the center of the YS at about 65 m depth). The power spectrum of this time series (Fig. 13a) shows that most of the peaks in the inflow position time series are also found in the spectrum of EOF mode 1 (Fig. 12a), including peaks at 34, 47, 60, 73, 93 and 171 days (the peaks of 256 and 341 days merge into one peak in both spectra). While the time series are not long enough for calculations of the significance and coherencies of the long-term peaks, which are the main interest here, a plot of both time series (Fig. 14) and direct linear regression calculation, with a correlation coefficient = 0.83, show that the two are correlated on short- and long-term periods. However, direct relation between the time evolution of mode 1 and eddy shedding events is not clear and their correlation is not statistically significant. Only two of the seven shed eddies seem to coincide with an eastward shift in the inflow, with the clearer example at the beginning of 1996 (Fig. 5), and possibly also in late 1994. An indirect effect of LC meander on eddy shedding is by its influence on the return transports (e.g., Fig. 5) and possibly also on the excitement of propagating meanders further north into the Gulf. As will be shown next, changes in inflow transport (which correlates with the return transport) do seem to affect eddy shedding.

EOF Mode 2- “the transport mode”. The spatial structure of mode 2 in Fig. 10 resembles the structure of the mean flow in the upper layers in Fig. 4a. This suggests that mode 2 may relate to the inflow transport in Fig. 8b. Indeed, the spectrum of the inflow transport (Fig. 13b) shows an energetic peak at 341 days, at the same period as the most energetic peak in mode 2. Fig. 15 compares the time evolution of mode 2 with the transport of the upper inflow. The correlation coefficient is 0.7 (A 30-day low pass filter

was applied in Fig. 15 to remove high frequencies. Without the filter, the correlation coefficient is smaller, 0.5, but is still significant at the 95% confidence level). Eddy shedding events are also marked in Fig. 15; almost all the eddy shedding events occurred when inflow transport has increased and is near its peak. One clear exception where the peak in transport is relatively small when an eddy was shed is at the beginning of 1996, which coincides with the extreme eastward shift in the inflow position and in the time evolution of EOF mode 1, as discussed before (Fig. 14). The fact that fluctuations in the inflow transport appear to correlate with eddy shedding events is perhaps not surprising, since each eddy shedding requires additional inflow transport to allow expansion of the LC. This result is also consistent with the correlation between LC extension and deep transport (Fig. 9), since in our model (as well as in Oey, 1996) the inflow and outflow transports are highly correlated with each other, but are in opposite directions.

EOF Modes 3 and 4- “the Maul’s modes”. We look at these two modes together, as these modes contain more variability near the deepest part at the center of the sill (mode 4 in particular) than the first two modes do. Modes 3 and 4 are compared with the model v-velocity component 150 m above the bottom at the center of our section. (The two modes seem to be out of phase with each other, as appear in their spatial structure, Fig. 10, and temporal evolution, Fig. 11, thus the combined time series is taken as $\Phi(t) = A_3\Phi_3(t) + A_4\Phi_4(t)$ with $(A_3, A_4) = (1, -1)$. The results below will eventually show that our choice of coefficients A_3 and A_4 was reasonable.) The linear regression correlation between modes 3 and 4 and the sill velocity, with correlation coefficient = 0.66, and the comparison of the two time series (Fig. 16), indicate that they correlate well. (A 30-day low pass filter was applied; without the filter the correlation coefficient is smaller, still significant = 0.44). Attempts to correlate each individual mode separately or use different coefficients A_i yield much lower correlations. Therefore, the combined modes 3 and 4 represent the dominant fluctuations in the deepest part of the channel. We will call these two modes “the Maul’s modes” because of their close relation with the sill velocity and

the apparent similarity in the time evolution of the two modes and the observed velocity. Moreover, the power spectrum of the combined record of modes 3 and 4 in Fig. 17 shows that the most energetic peak is at 205 day- the same period as the model and the Maul's observed spectra of Fig. 3. Because the lower EOF modes are independent from the first two modes, which more directly relate to variations in upper channel transport and LC extension, it may be difficult to find significant correlations between sill velocity and LC extension (i.e., Maul et al., 1985).

4. Summary and conclusions

Recent observations (Bunge et al., 2001; Ochoa et al., 2001; Sheinbaum et al., 2002) indicate more complex flow field and variability than previously thought based on more limited measurements (Maul, 1977; Maul et al., 1985; Burkov et al., 1982). However, little is known about the nature of the forcing and the physical parameters that account for their variability. The aim of the study is therefore to analyze results from a high resolution numerical ocean model in order to describe the structure and variability of the flow through the YS, and to better understand how these relate to the forcing of LC variations and eddy shedding. The analysis of model results includes two parts. In the first part, a comparison was made between model results and published observations, in order to evaluate the overall statistics, e.g., mean and standard deviation of velocity and transports, of the flow. In the second part an EOF and coherency analysis were made in an attempt to identify the forcing and physical parameters responsible for the dominant modal fluctuations in the Strait.

The model results indicate a highly variable flow field through the YS, which agrees with observations in most aspects. The results show a complex structure in the flow field with four distinct major cores: 1. An upper ocean inflow core with transport of 33 Sv and maximum mean flow of about 1.5 m s^{-1} , which located near the western

(Mexican) side of the YS, but occasionally shifts offshore on time scales of about 6 months. 2. An upper ocean recirculation outflow core with transport of about 5.5 Sv and maximum mean flow of about 0.25 m s^{-1} , which is located near the eastern (Cuban) side of the YS. 3. A deep boundary undercurrent along the western slope with mean southward velocity of 0.17 m s^{-1} . 4. A deep boundary undercurrent along the eastern slope with mean southward velocity of 0.1 m s^{-1} . The total deep return currents combined to an outflow mean transport of about 2.5 Sv, but occasionally return deep transports are as large as 5-10 Sv. One discrepancy between the model results and the new observations (Ochoa et al., 2001; Sheinbaum et al., 2002) is that, the model shows a more extended return flow near the surface on the eastern side of the strait than the observations do. Because of the large interannual variability of the flow in this area, and the limited period of observations (<2 years) a much longer observed record is probably needed in order to verify the exact nature of this feature. Simulations with data assimilation during the period coincident with that observed (Oey et al., 2002; Wang et al., 2002) do indicate a weaker eastern return flow, more similar to the observations. On the other hand, the total net transport across the strait in the present model, 25.3 Sv, is in good agreement with recent observed estimates of a mean transport of 25 Sv (Ochoa et al., 2001) or 23.8 (Sheinbaum et al., 2002). Previous estimates in the YS sited a larger mean transport of 28-30 Sv (Schmitz and Richardson, 1991; Schmitz and McCartney, 1993; Johns et al., 2002).

When the LC volume increases the upper inflow increases, and thus the deep return flow must increase, as proposed by Maul (1977), Maul et al. (1985), and recently observed by Bunge et al. (2001). This relation is confirmed in our calculations- a significant linear correlation was found between changes in the extension of the LC and the total deep return flow below 800 m. Pulses of strong return deep flows coincide with large increase in LC volume; such pulses usually occur between eddy shedding events when the LC is growing and are mostly confined to the west and east deep slopes of the

channel. The results are consistent with the early simulations using a smaller domain (Oey, 1996), thus suggesting that the inflow/outflow relation in the YS is largely controlled by local dynamics.

An EOF analysis explores the spatial structure of the first four modes and their temporal evolution. The first four EOF modes accounts for 50%, 18%, 11% and 7%, respectively, of the variability. The EOF mode#1 of the along-strait currents is surface-trapped, is 180° out of phase across the channel, and correlates well (correlation coefficient $\gamma \approx 0.8$) with the cross-channel vacillations of the LC frontal position. Its time-series at times visually correlates also with the inflow transport and LC eddy-shedding events (e.g., Fig. 5) but the correlation is not statistically significant. The EOF mode#2 has a spatial structure that mimics that of the mean flow: dominated by two vertically more coherent regions that are 180° out of phase across the Strait. The mode is dominated by two periods, approximately 11 months and 2 months respectively, and correlates ($\gamma \approx 0.7$) with the inflow transport. This mode seems to directly relate to eddy shedding events; six of the seven eddies shed during the 4-year simulation occurred near a peak in the inflow transport, the seventh eddy shed near a peak in mode#1 and an extreme eastward shift in the position of the inflow. The time-series of the combined EOF mode#3 and mode#4 together correlates ($\gamma \approx 0.66$) with the deep current over the sill, and is dominated by fluctuations with a period ≈ 205 days coincident with the dominant low-frequency fluctuations inherent in Maul et al.'s (1985) sill measurement. The lower modes (#3 and #4) account for most of the velocity variability in the deep layers over the center of the sill.

Following the above description of the EOF modes in the Yucatan Straits, we suggest naming these EOF modes “the meander mode” (mode 1), “the transport mode” (mode 2), and “the Maul’s modes” (modes 3 and 4). While we clearly identified the long-term modes of variability, more analysis is needed to understand the various high frequency oscillations evident in the observed and the simulated records.

Our results may help to explain why Maul et al. (1985) could not find a significant correlation between the near-bottom velocity at the center of the sill and variations in the LC expansion. First, the location of the Maul's current meter was at the center of the sill while most of the deep outflow (in the model and in the new observations) is on the side slopes of the channel. Second, the so-called "Maul's mode" (EOF modes 3 and 4) do not correlate with the LC meander mode (EOF mode 1), nor with the transport mode (EOF mode 2).

An important question is whether or not variations in the YS flow affect the frequency of LC eddy shedding. Do the most energetic peaks in the YS EOF modes, 5.6 months, 8.4 months and 11.2 months, relate to the frequency of LC eddy shedding?. Unfortunately, our simulations are not long enough to obtain a reliable statistics of eddy shedding frequency in the model, as has been done by Sturges and Leben (2000) from analysis of 27 years of observations which show dominant eddy shedding frequencies of 6, 9 and 11 months. During the four-year period analyzed here, seven LC eddies were shed at irregular time intervals of 6.6, 7.1, 5.3, 11.9, 4.2 and 10.9 months, thus suggesting that there is a relation between the EOF modes and eddy shedding events. This relation has been established to some extent for the EOF mode#2 and the variations in the inflow transport, but it is less clear for other modes.

That the present simulation gives irregular LCE-shedding periods is significant. Oey (1996) shows such irregular shedding periods only when horizontal viscosity in a coarser resolution model was reduced. In a separate simulation with the same model used here, but without wind (Oey et al., 2002; Lee and Oey, 2002) a *regular* LCE-shedding ensue. The results presented her, thus offer an additional mechanism by which irregular shedding can occur as a result of fluctuating YS transports forced by the wind. Therefore, while the basic dynamics in the YS may be controlled internally by local topography and stratification, wind (local and remote) can play an important role in affecting LC and eddy shedding frequency.

Acknowledgements. The study is supported by the Mineral Management Service under contracts# 1435-01-00-CT-31076 and 01-99-CT-31028 (via SAIC). T.E is also supported by the Office of Naval Research, award# N00014-00-1-0228. Computational resources were provided by the NOAA/GFDL super computer facilities.

REFERENCES

- Baringer, M. O. and J. C. Larsen, Sixteen years of Florida Current transport at 27°N, *Geop. Res. Let.*, 28, 3179-3182, 2001.
- Blumberg, A. F. and G. L. Mellor, A description of a three-dimensional coastal ocean circulation model, in *Three-Dimensional Coastal ocean Models, Coastal Estuarine Stud.*, vol. 4, edited by N. S. Heaps, 1-16, AGU, Washington, DC., 1987.
- Bretherton, C. S., C. Smith and J. M. Wallace, An intercomparison of methods for finding coupled patterns in climate data, *J. Clim.*, 5, 541-560, 1992.
- Bunge, L., J. Ochoa, A. Badan, J. Candela and J. Sheinbaum, Deep flows in the Yucatan Channel and their relation to changes in the Loop Current extension, *J. Geophys. Res.*, Submitted. (2001)
- Burkov, V. A., L. I. Galerkin and A. B. Zubin, New data on water exchange through the Yucatan Strait (in Russian), *Dokl. Akade. Nauk USSR*, 265, 190-195, 1982. [Available as a translation from *Oceanology*, 198-200, 1984.]
- Hurlburt, H. E. and J. D. Thompson, A numerical study of Loop Current intrusions and eddy shedding, *J. Phys. Oceanogr.*, 10, 1611-1651, 1980.
- Johns, W. E., T. L. Townsend, D. M. Fratanton and W. D. Wilson, On the Atlantic inflow to the Caribbean Sea. *Deep-Sea Res.*, 49, 211-243, 2002.
- Maul, G. A. The annual cycle of the Gulf Loop Current. Part I: Observations during a one-year time series, *J. Mar. Res.*, 35, 29-47, 1977.

- Maul, G. A., D. A. Mayer and S. R. Baig, Comparisons between a continuous 3-year current-meter observation at the sill of the Yucatan Strait, satellite measurements of Gulf Loop Current area, and regional sea level, *J. Geophys. Res.*, 90, 9089-9096, 1985.
- Mellor, G. L., Users guide for a three-dimensional, primitive equation, numerical ocean model, Program in Atmospheric and Oceanic Sciences, Princeton University, 38 pp, 1996.
- Lee, H.-C. and L.-Y. Oey, The relation between the Loop Current variability and the Caribbean Sea dynamics, to be submitted, 2002.
- Ochoa, J., J. Sheinbaum, A. Baden, J. Candela and D. Wilson, Geostrophy via Potential vorticity inversion in the Yucatan Channel, *J. Mar. Res.*, 59, 725-747, 2001.
- Oey, L.-Y., Simulation of mesoscale variability in the Gulf of Mexico: Sensitivity studies, comparison with observations, and trapped wave propagation, *J. Phys. Oceanogr.*, 26, 145-175, 1996.
- Oey, L.-Y. and P. Chen, A model simulation of circulation in the north-east Atlantic shelves and seas, *J. Geophys. Res.*, 97, 20,087-20,115, 1992.
- Oey, L.-Y. and H.-C. Lee, Deep energetics and topographic Rossby waves in the Gulf of Mexico, *J. Phys. Oceanogr.*, Submitted, 2001.
- Oey, L.-Y., H.-C. Lee and T. Ezer, An embedded circulation model of the Gulf of Mexico Part I: Descriptions and experiments using ECMWF winds and satellite data, to be submitted, 2002.
- Schmitz, W. J., Jr. and M. S. McCartney, On the North Atlantic circulation, *Rev. Geophys.*, 31, 29-49, 1993.
- Schmitz, W. J., Jr. and P. L. Richardson On the sources of the Florida Current. *Deep-Sea Res.*, 38, Suppl. #1, 379-409, 1991.
- Sheinbaum, J., J. Candela, A. Badan and J. Ochoa, Flow structure and transports in the Yucatan Channel, *Geophys. Res. Lett.*, 29(3), 10.1029/2001GL0139990, 2002.

- Sturges, W., The frequency of ring separations from the Loop Current, *J. Phys. Oceanogr.*, 24, 1647-1651, 1993.
- Sturges, W. and R. Leben, Frequency of ring separations from the Loop Current
In the Gulf of Mexico: A revised estimate, *J. Phys. Oceanogr.*, 30, 1814-1818, 2000.
- Sturges, W., J. C. Evans, W. Holland and S. Welsh, Separation of warm-core rings
in the Gulf of Mexico, *J. Phys. Oceanogr.*, 23, 250-268, 1993.
- Teague, W. J., M. J. Carron and P. J. Hogan, A comparison between the Generalized
Digital Environmental Model and Levitus climatologies, *J. Geophys. Res.* 95, 7167-
7183, 1990.
- Wang, D.-P., L.-Y. Oey, T. Ezer and P. Hamilton, The near-surface currents in DeSoto
Canyon (1997-1999): Observations, satellite data, and comparison with model
simulations, *J. Phys. Oceanogr.*, Submitted, 2002.
- Welsh, S. E. and M. Inoue Loop Current rings and the deep circulation in the Gulf
of Mexico, *J. Geophys. Res.*, 105, 16,951-16,959, 2000.

Figure Captions

Figure 1. Bottom topography and main features of the study area (the model domain extends beyond the shown area, see text). Topographic contour interval is 100 m for areas shallower than 500 m, and 500 m elsewhere. The Caribbean Sea (CS), the Gulf of Mexico (GOM), the Loop Current (LC), the Florida Straits (FS) and the Yucatan Strait (YS) are indicated. The location of the Maul et al. (1985) observed time series of Fig. 2 is marked by “M”; The YS model cross section of Fig. 4 is marked by the solid line. The box around the LC indicates the area in which sea surface height was averaged in Fig. 8a.

Figure 2. Comparison between the observed flow above the sill of the Yucatan Strait, at 1895 m depth (Maul et al., 1985), (left panels), and model calculations (right panels). Across channel (east-west, u-component) and along channel (north-south, v-component) are shown in the upper and lower panels, respectively; average and standard deviation are indicated in each panel. Observed daily averages are shown from November 1977 to October 1980, and model daily averages are shown from November 1992 to October 1995.

Figure 3. Power spectra of, (a) observed, and (b) model, v component records of Fig. 2. The periods (in days) of the most energetic peaks are indicated.

Figure 4. (a) Mean v-component velocity across the section shown in Fig. 1, and calculated from the model simulations of 1993-1996. Shaded region and dashed lines indicate negative values, i.e., from the GOM into the Caribbean Sea. (b) Standard deviation across the Yucatan Strait. Contour intervals are 0.05/0.1 m s⁻¹ in (a) for negative/positive values, and 0.01/0.04 m s⁻¹ in (b) for values below/above 0.1 m s⁻¹.

Figure 5. Variations in along-channel flow across the Yucatan Strait during an eddy shedding event. Surface elevation contours are shown in the left-bottom corner of each panel. Panels (a) to (f) are daily averages in 20-day intervals. Contours and shading are as in Fig. 4.

Figure 6. Velocity vectors in the YS region on model day 1 December, 1995 (corresponding to Fig. 5c): (a) velocity at the sixth sigma level from the surface layer (over the YS sill this level is at a depth of about 65 m), and (b) velocity at the sixth sigma level from the bottom layer (over the YS sill this level is about 65 m from the bottom). Light and dark gray shading represent bottom depths of 2000 m – 3000 m and above 3000 m, respectively. The location of the Maul’s current meter is indicated by “M”.

Figure 7. Velocity vectors as in Fig. 6, but for model day 10 January, 1996 (corresponding to Fig. 5e).

Figure 8. (a) Variations of area averaged surface elevation over the Loop Current region shown in Fig. 1 and eddy shedding events (marked by “E”s). (b) Variations of daily inflow transport above 800 m (solid line), and total net transport across the Yucatan Strait (dashed line). (c) Variations of daily outflow transport below 800 m (solid line) and outflow transport above 800 m (dashed line).

Figure 9. Outflow transport below 800 m (solid line, in Sv) and area averaged surface elevation change (dashed line, in cm change per 10 days). Both time series were smoothed by a 30-days low-pass filter. Correlation coefficient is -0.4.

Figure 10. The spatial structure of the first four Empirical Orthogonal Modes (EOF) of the along-channel flow (the percent of variability represented by each mode is indicated in parentheses). Shaded areas and dashed contours represent negative values; each contour represents 1/100th of a normalized amplitude value.

Figure 11. The temporal variations of the first four EOF Modes shown in Fig. 10.

Figure 12. Power spectra of the time evolution of the first four EOF Modes shown in Fig. 11. The period (in days) of the most energetic peaks are indicated.

Figure 13. Power spectra of (a) the east-west variation in the position of the inflow core defined by the location of the 40 cm^{-1} contour at sigma level 6 (about 50 m below the surface, see Fig. 4), and (b) the inflow transport (the solid line in Fig. 8b). The period (in days) of the most energetic peaks are indicated.

Figure 14. A comparison of the east-west variations in the position of the inflow core across the YS, defined by the location of the 40 cm s^{-1} contour at the sixth sigma level (solid line) and the time evolution of EOF mode 1 (dashed line). The amplitude of the EOF mode (see Fig. 11a) is scaled to fit the longitude units of the flow position. The linear regression correlation coefficient is 0.83.

Figure 15. A comparison of the variations in the transport of the inflow core (the solid line of Fig. 8b) (solid line) and the time evolution of EOF mode 2 (dashed line). The amplitude of the EOF mode (see Fig. 11b) is scaled to fit the units (Sv) of the transport. The time series were smoothed with a 30-day low pass filter. The linear regression correlation coefficient is 0.7.

Figure 16. A comparison of the model v-velocity component at the center of the section in Fig. 4, at 150 m above the sill depth (solid line), and the sum of mode 3 and mode 4 (dashed line). The sign of mode 4 has been reversed and the amplitude of the sum of the modes was scaled to fit the units and sign of the velocity record. The time series were smoothed with a 30-day low pass. The linear regression correlation coefficient is 0.66.

Figure 17. Power spectrum of the combined time evolution record of EOF modes 3 and 4 (unsmoothed). The period (in days) of the most energetic peaks are indicated. Note that the 205 days peak of the observed and model deep velocity over the sill (Fig. 3) is reproduced by the combined EOF modes.

Fig. 1

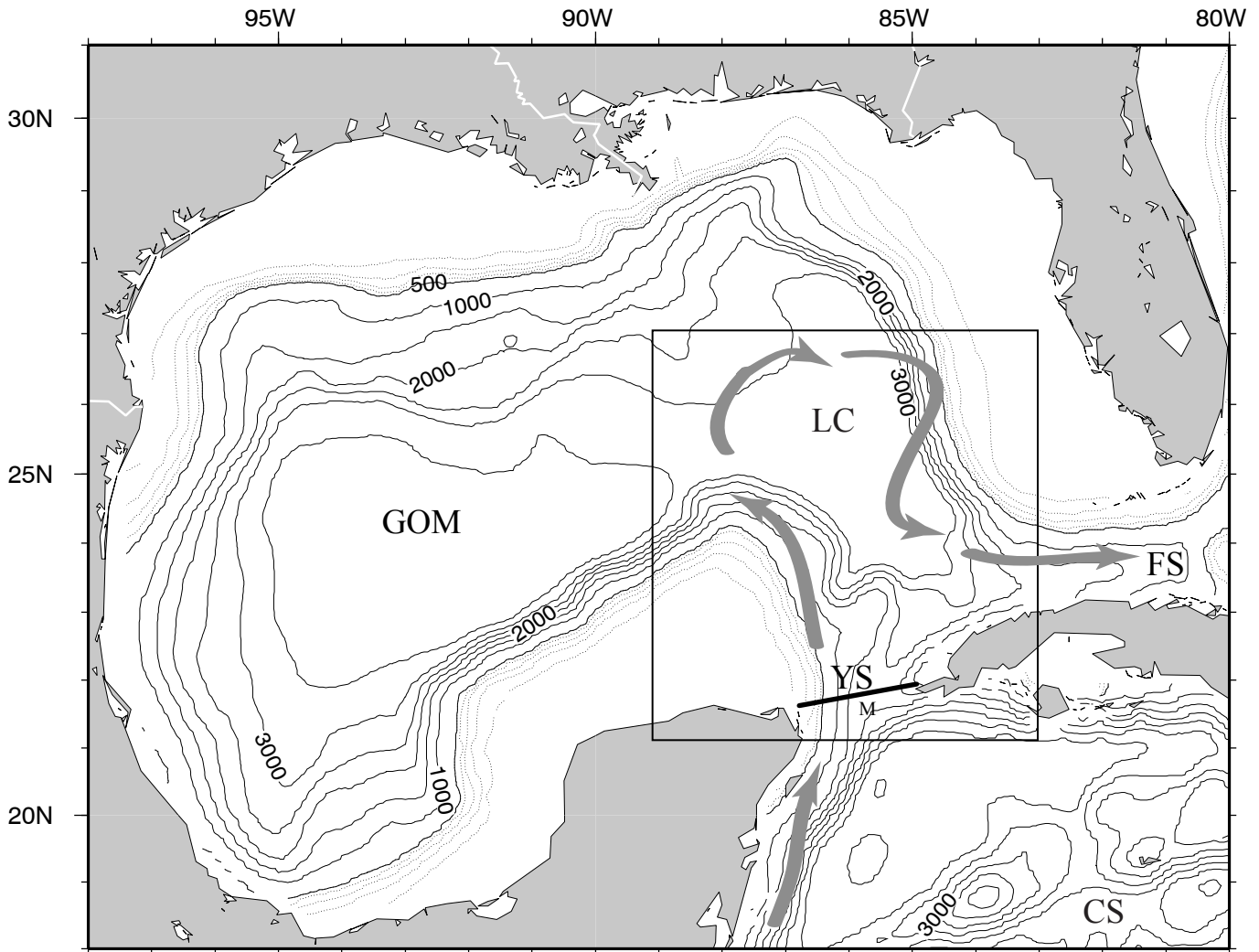


Fig. 2

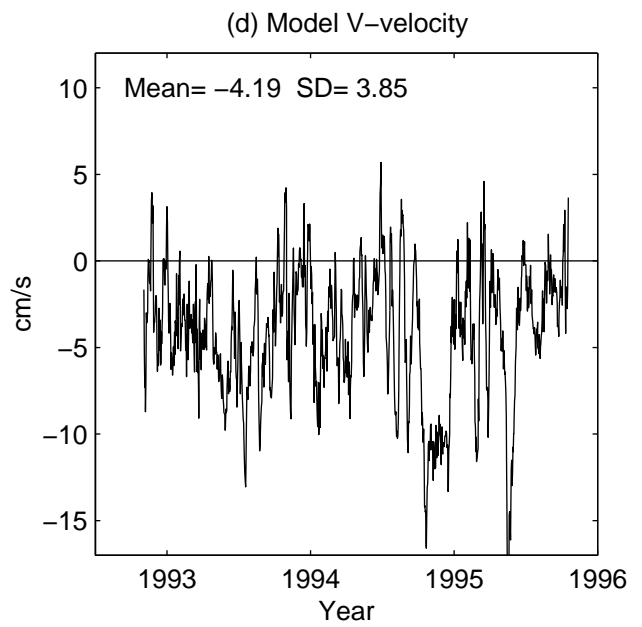
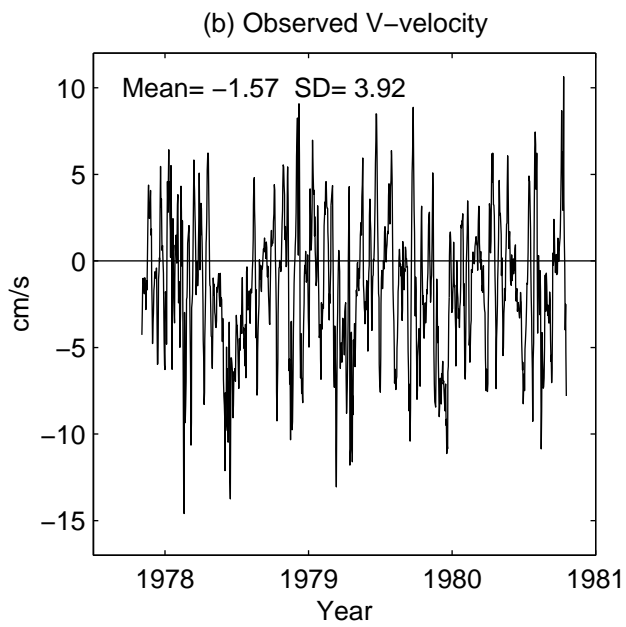
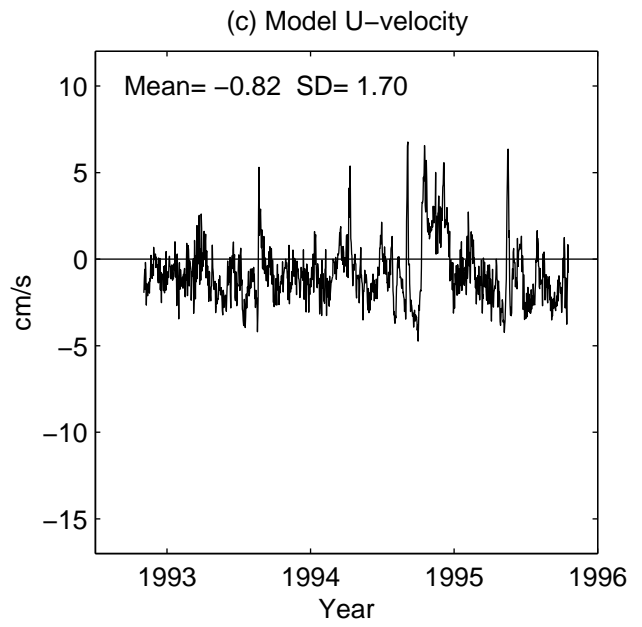
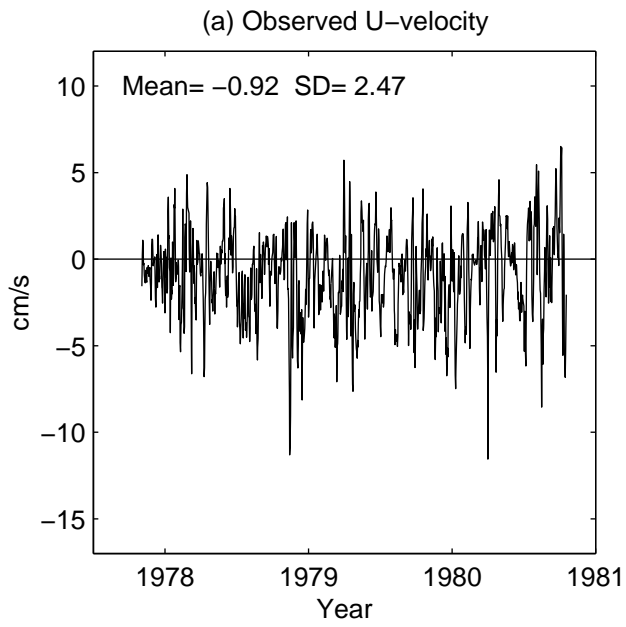


Fig. 3

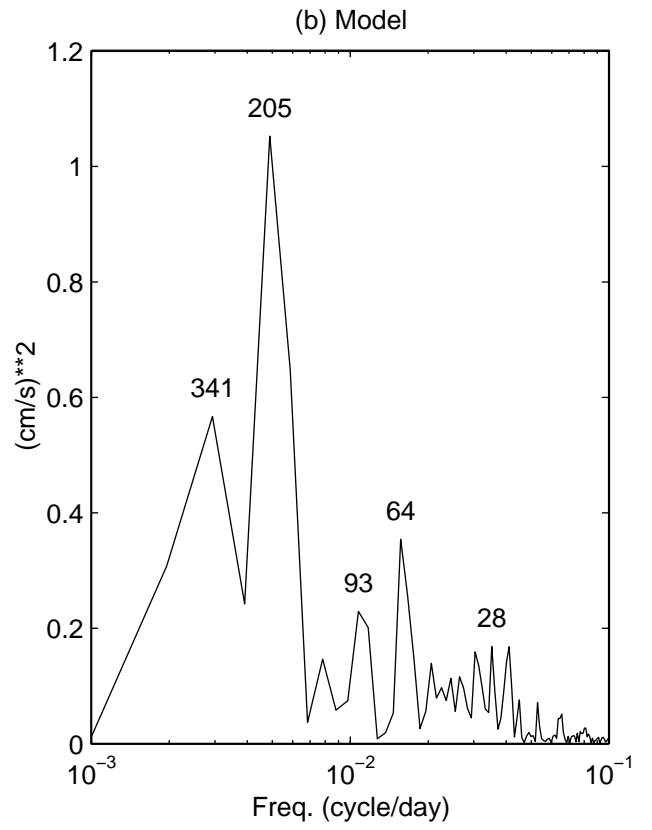
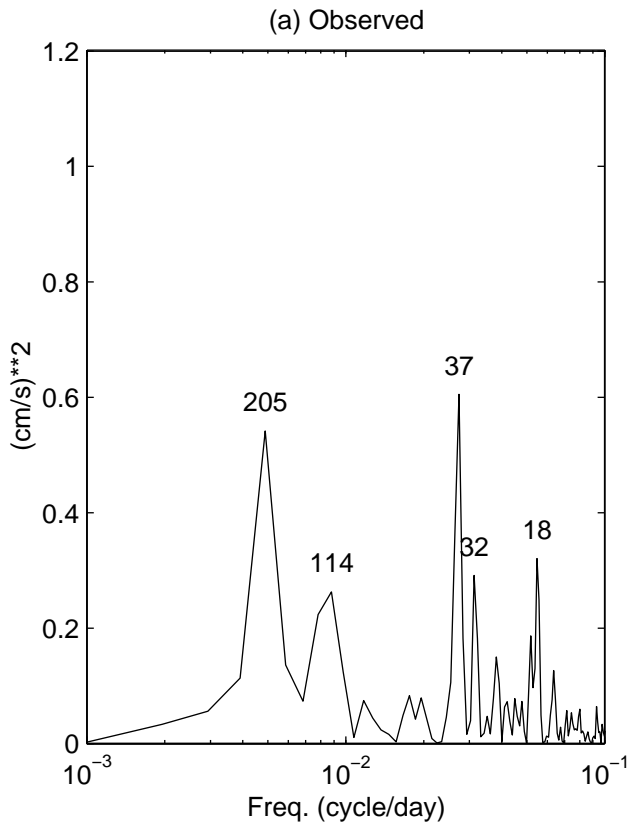


Fig. 4

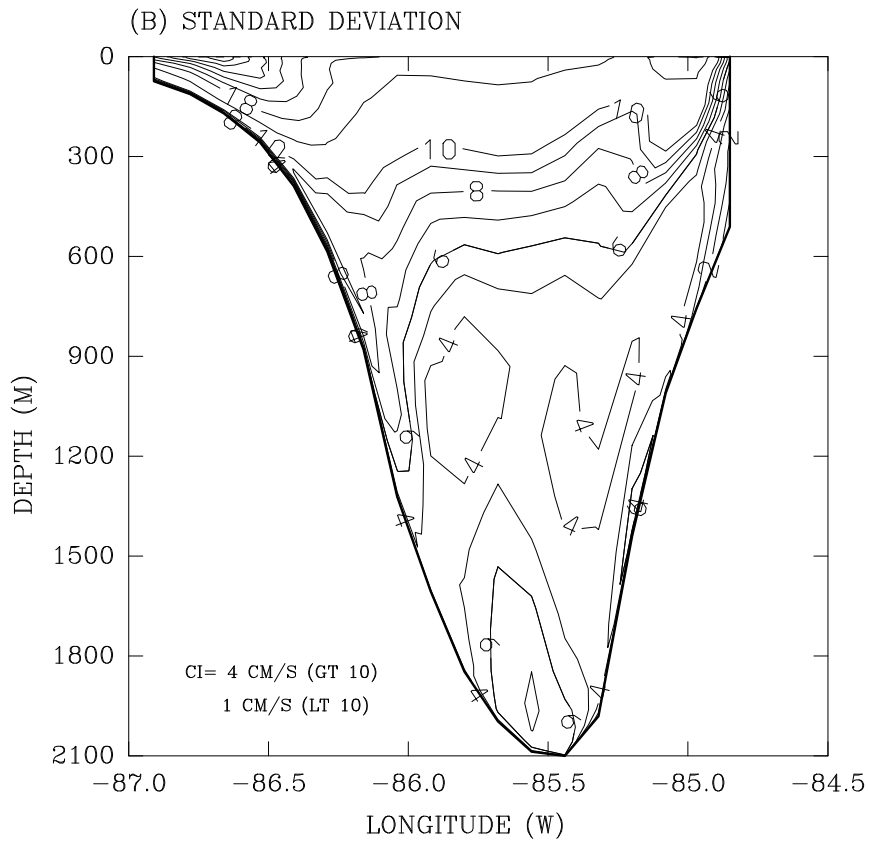
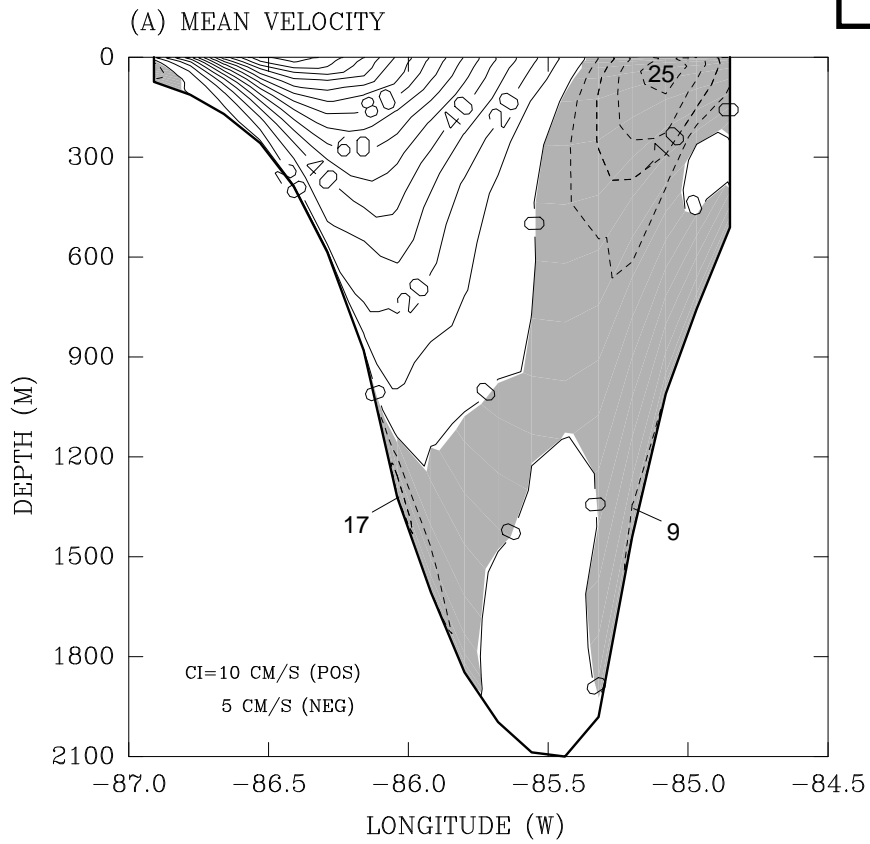
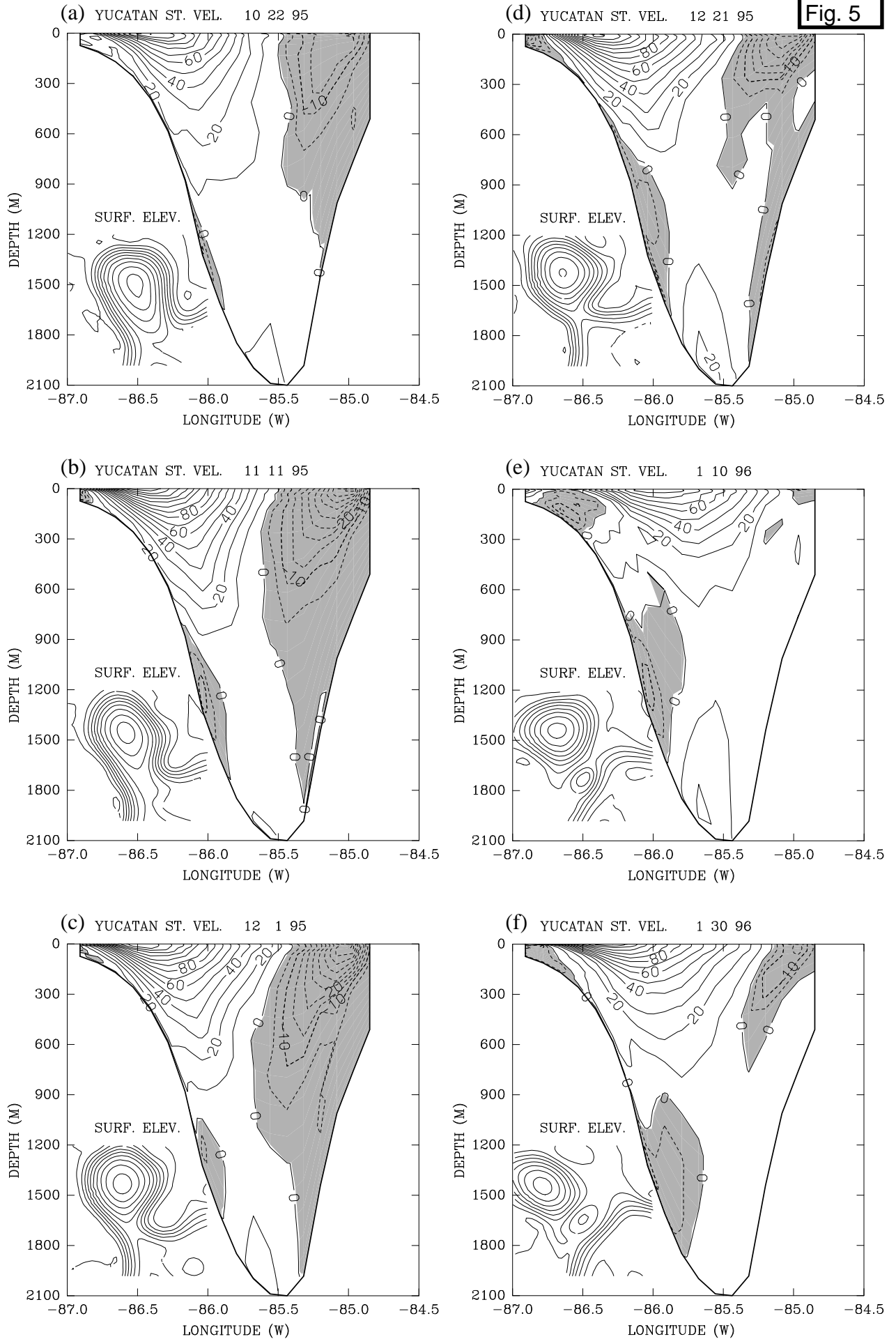


Fig. 5



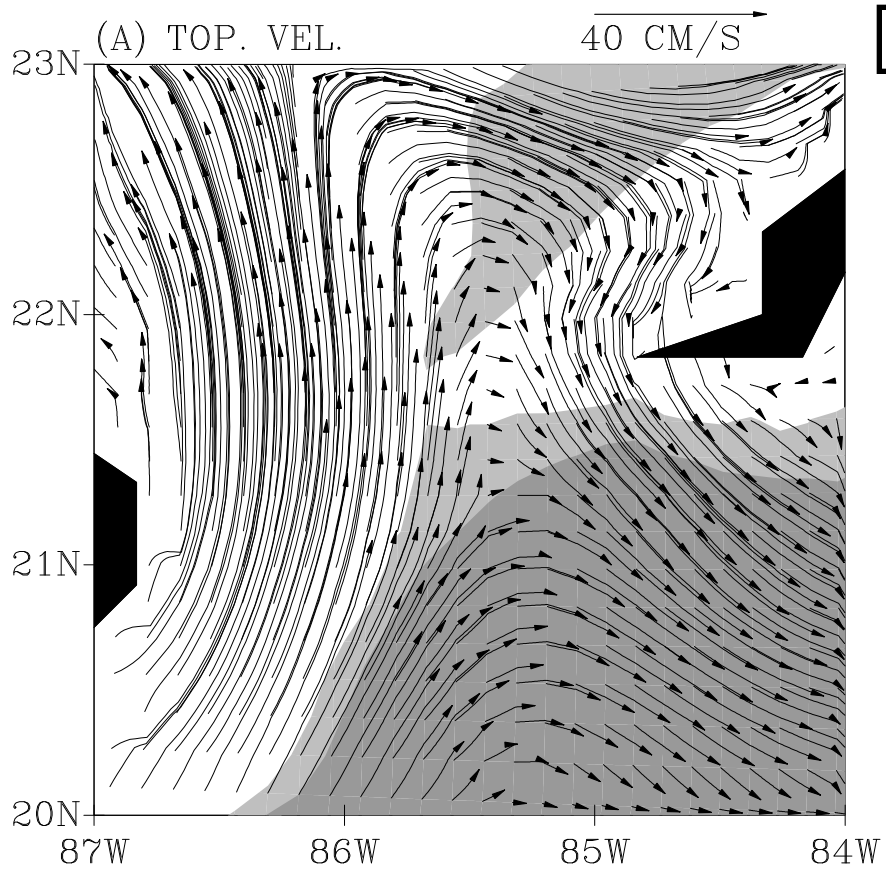


Fig. 6

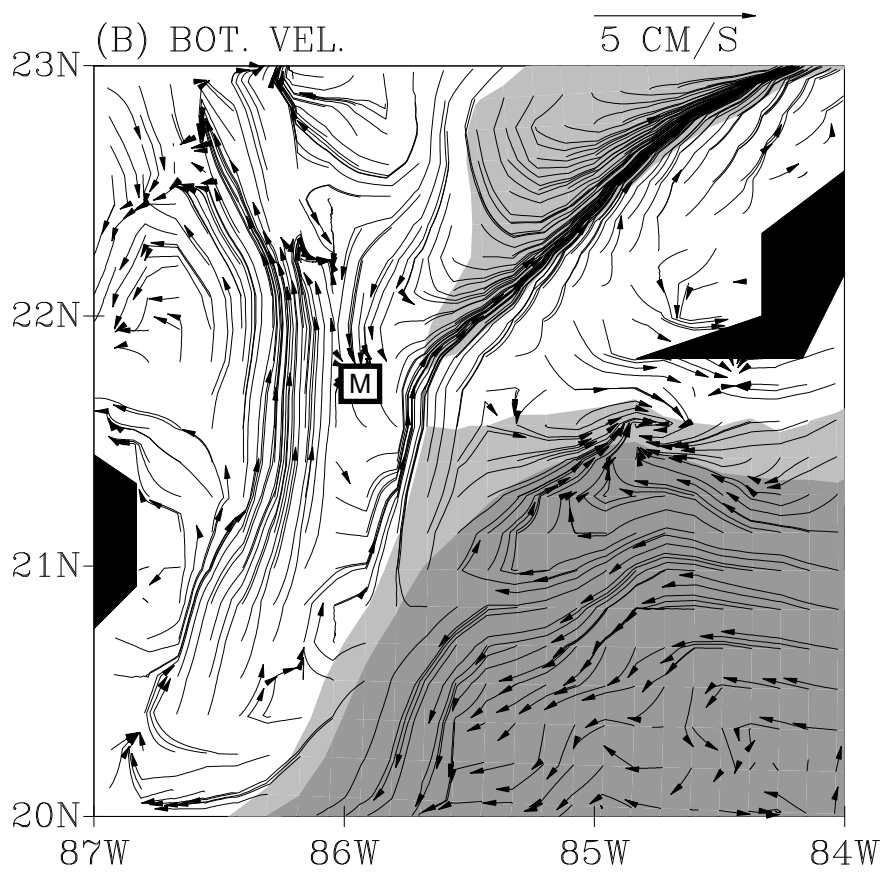


Fig. 7

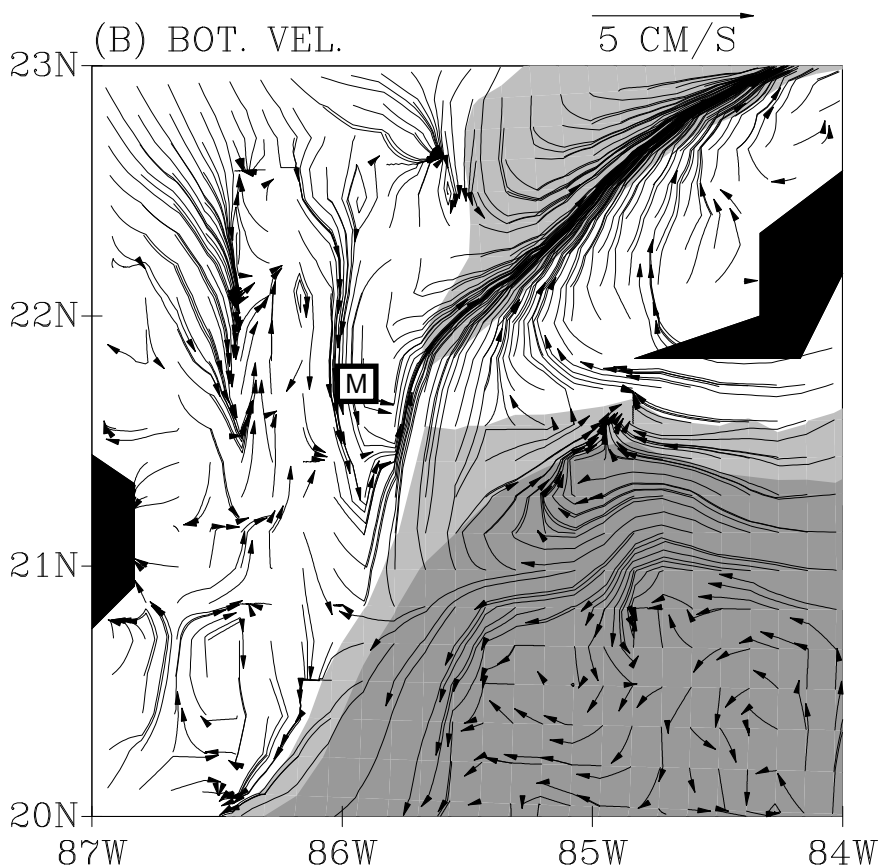
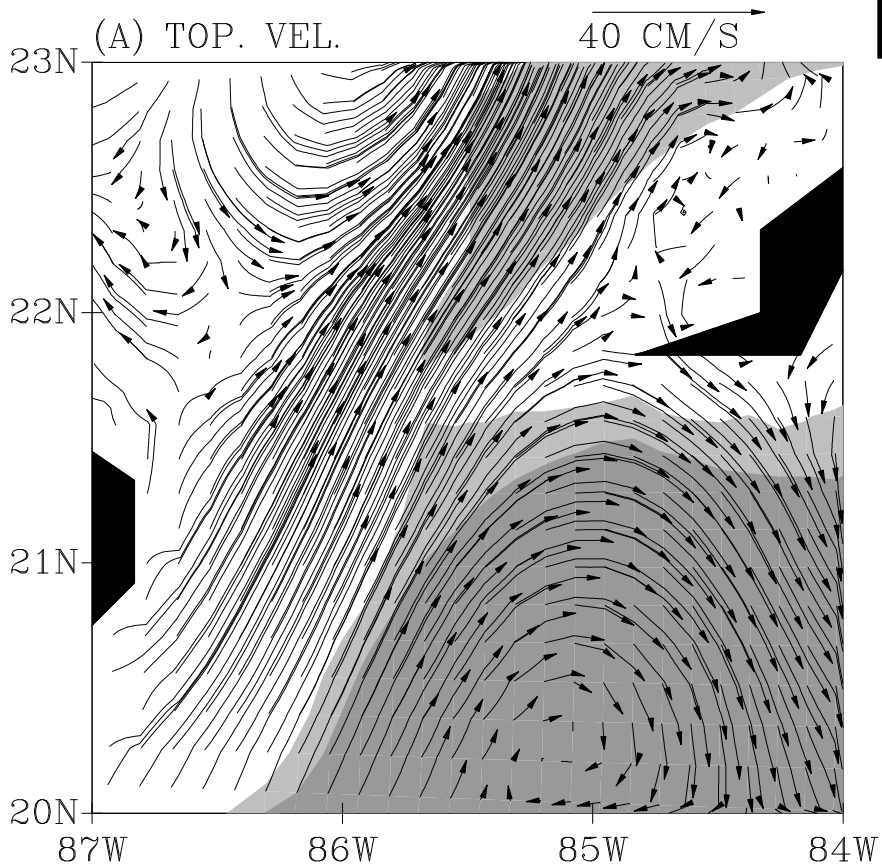
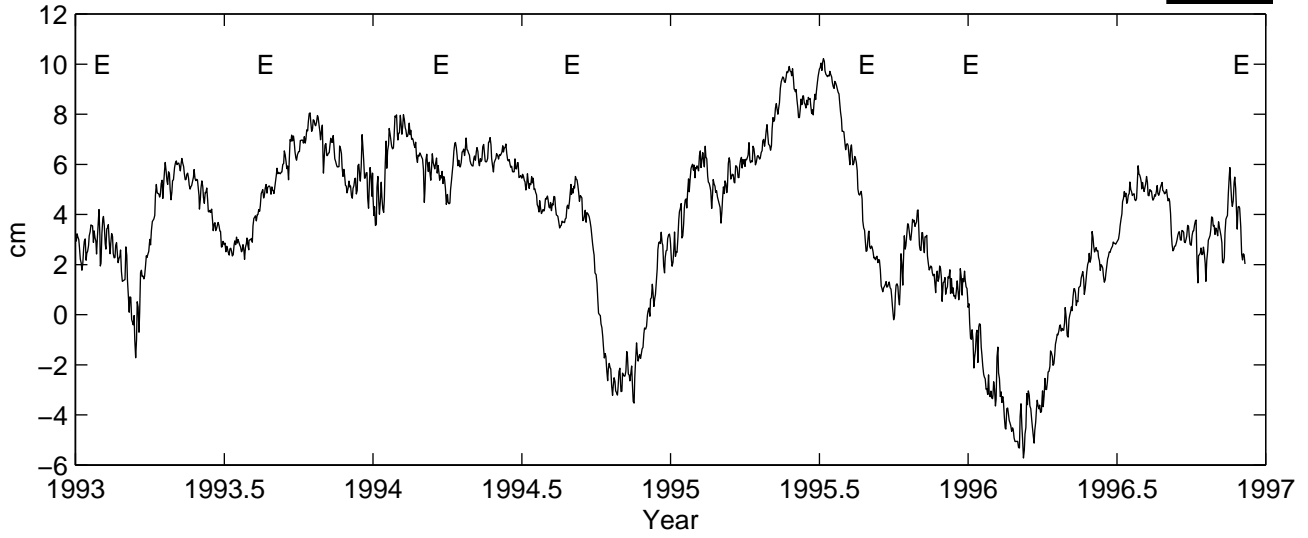
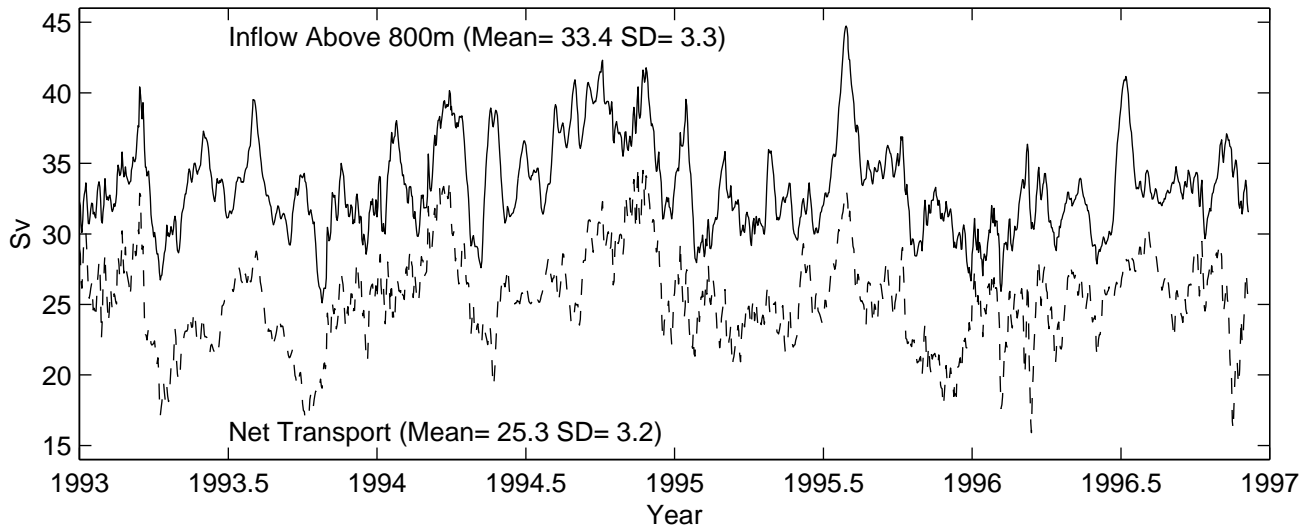


Fig. 8

(a) Mean Surf. Elev. and Eddies Shed



(b) Inflow Transport



(c) Outflow Transport

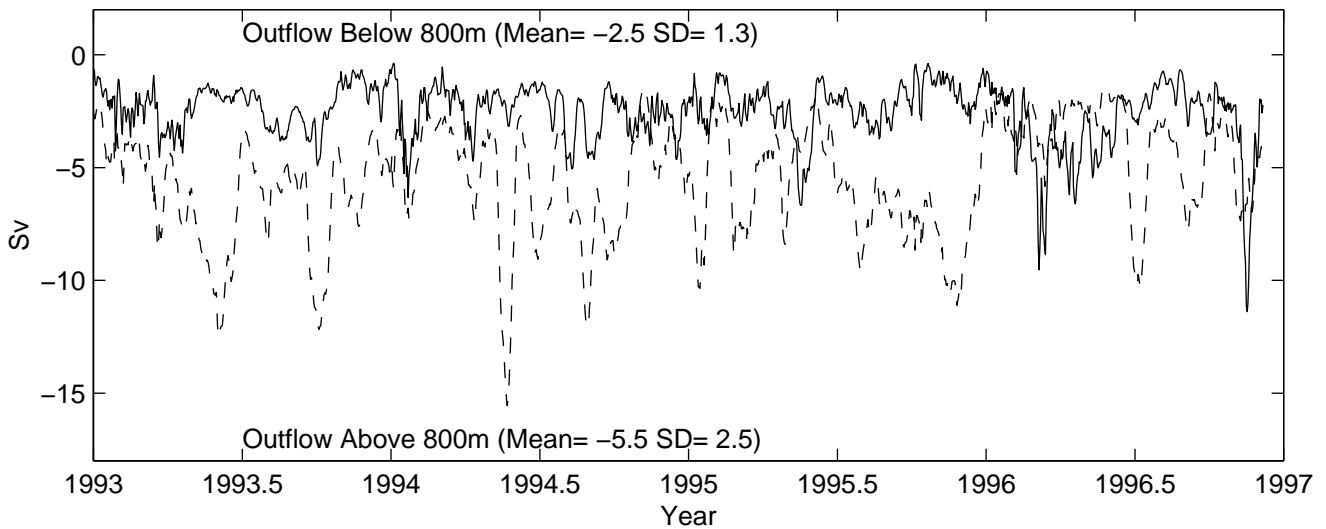


Fig. 9

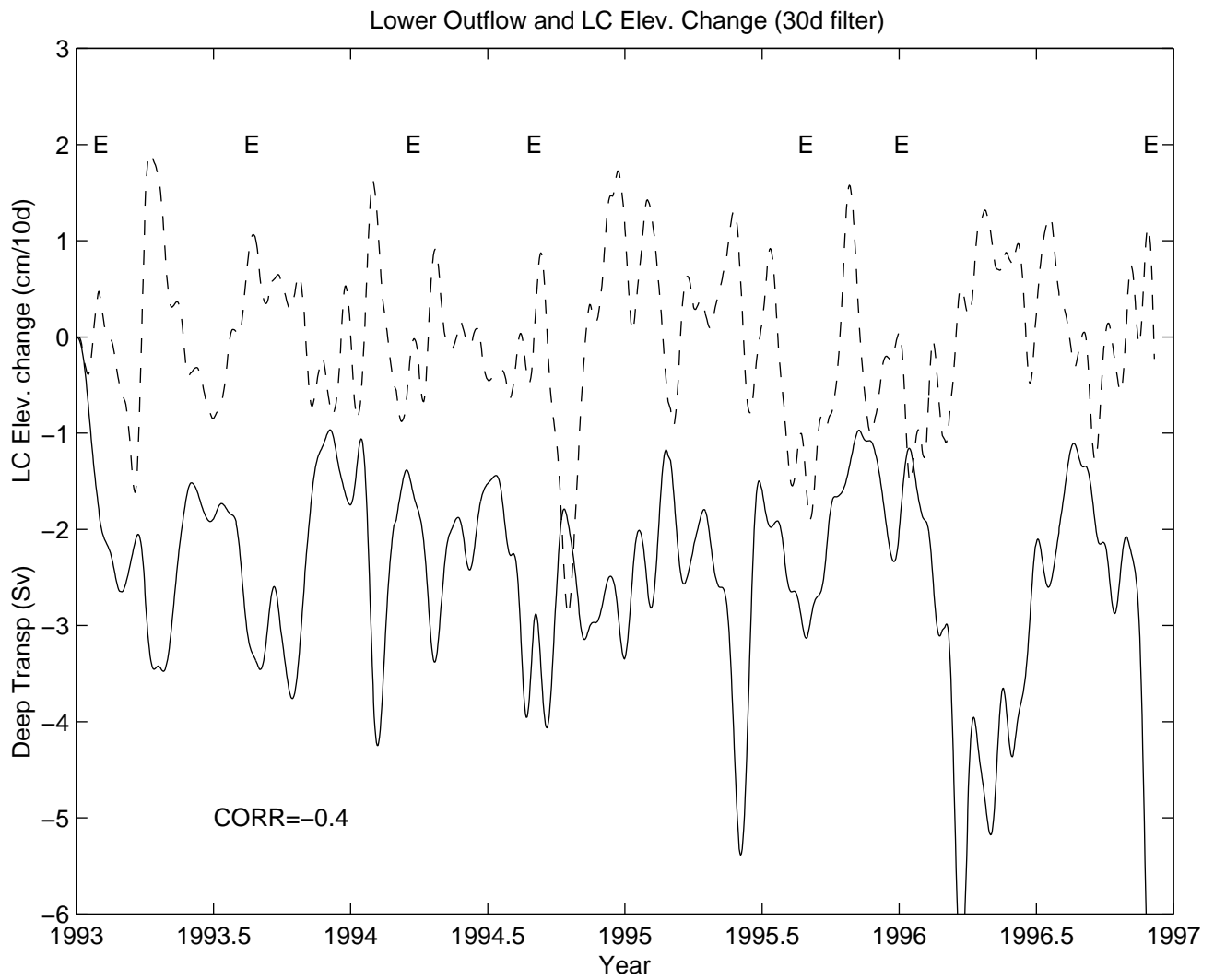


Fig. 10

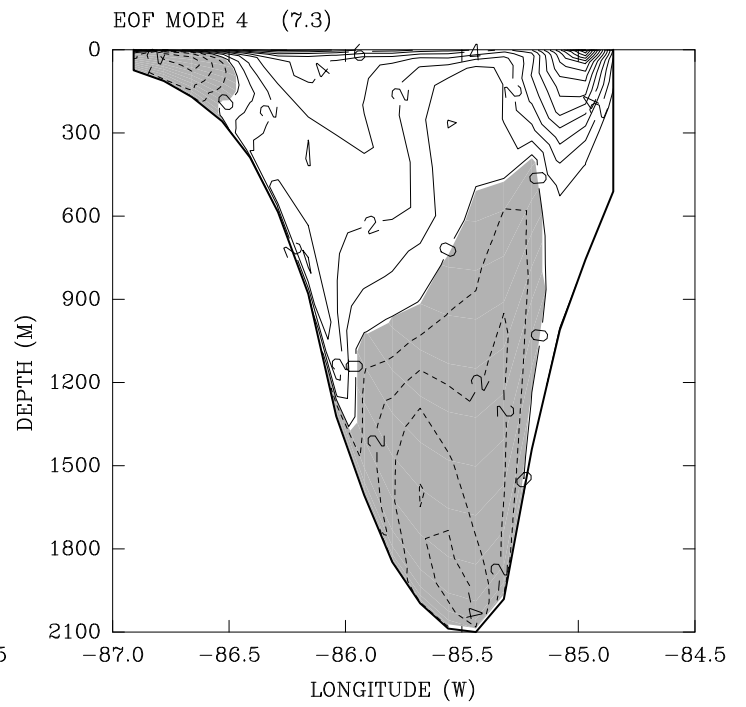
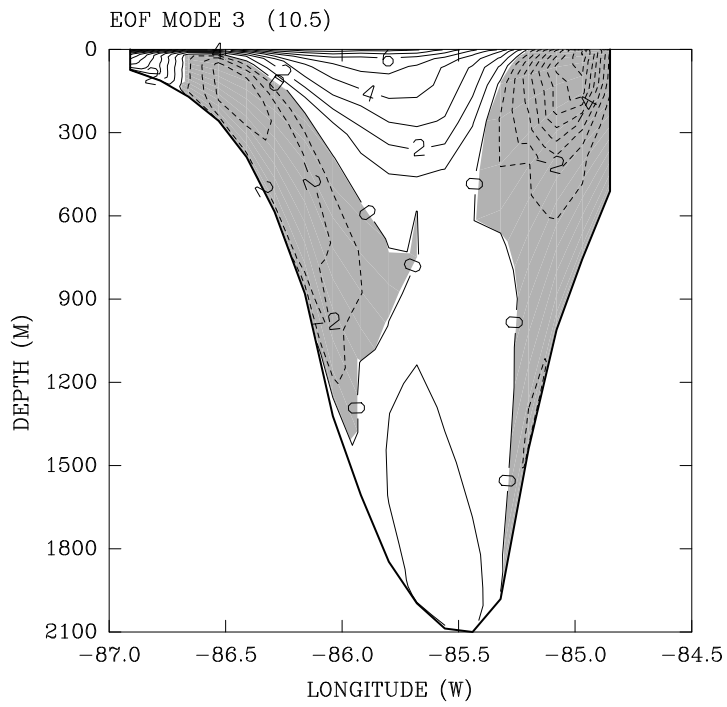
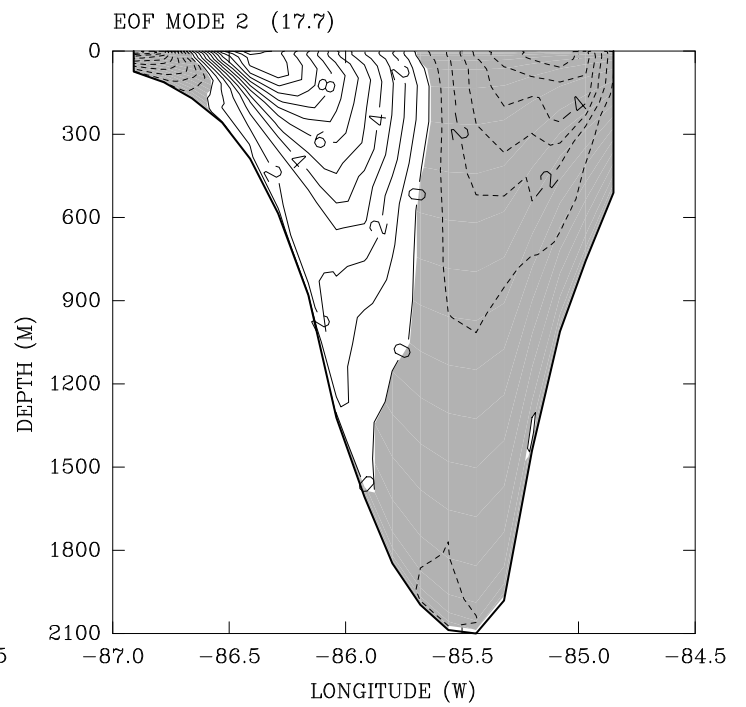
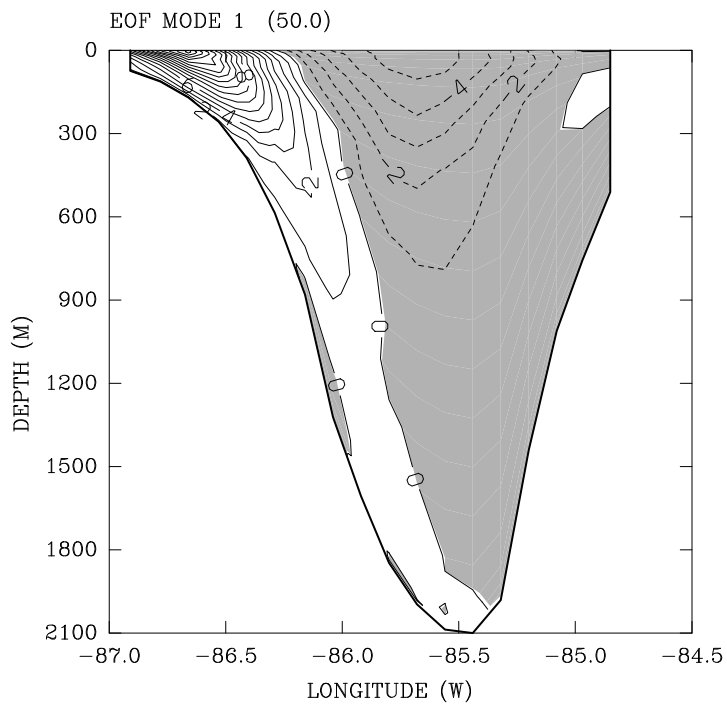


Fig. 11

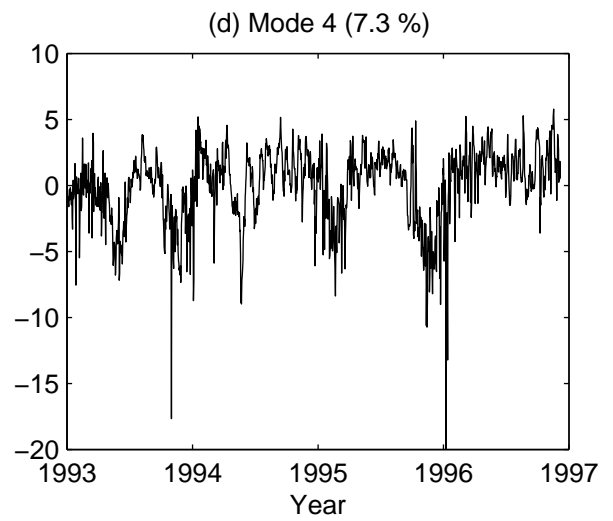
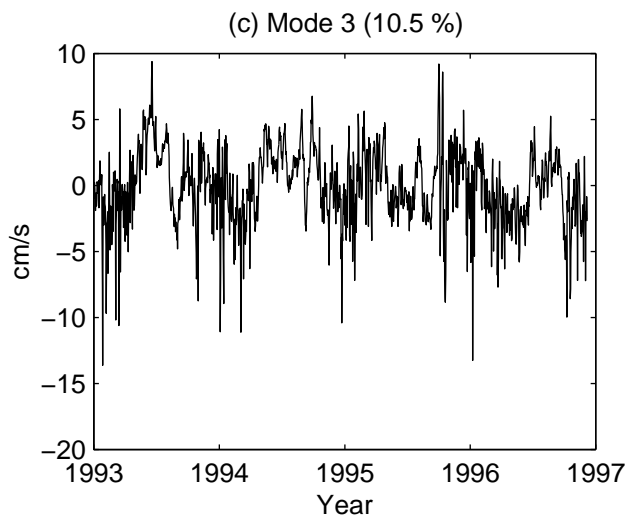
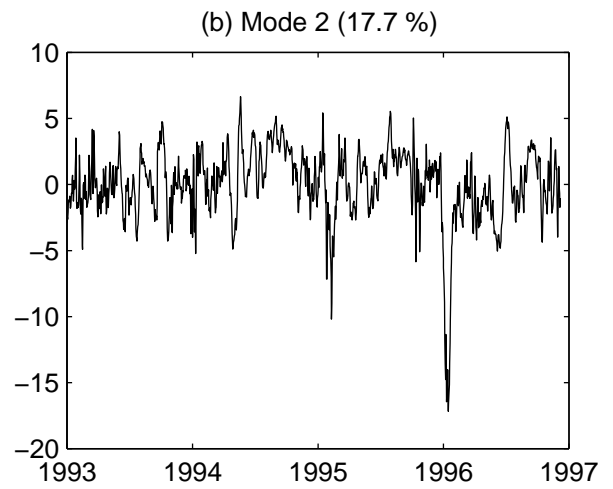
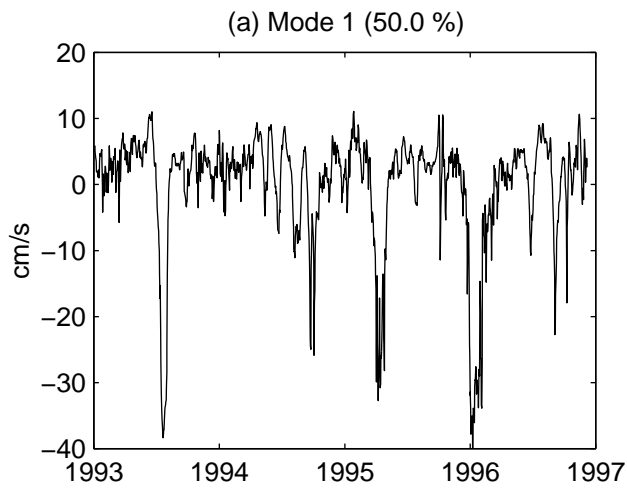


Fig. 12

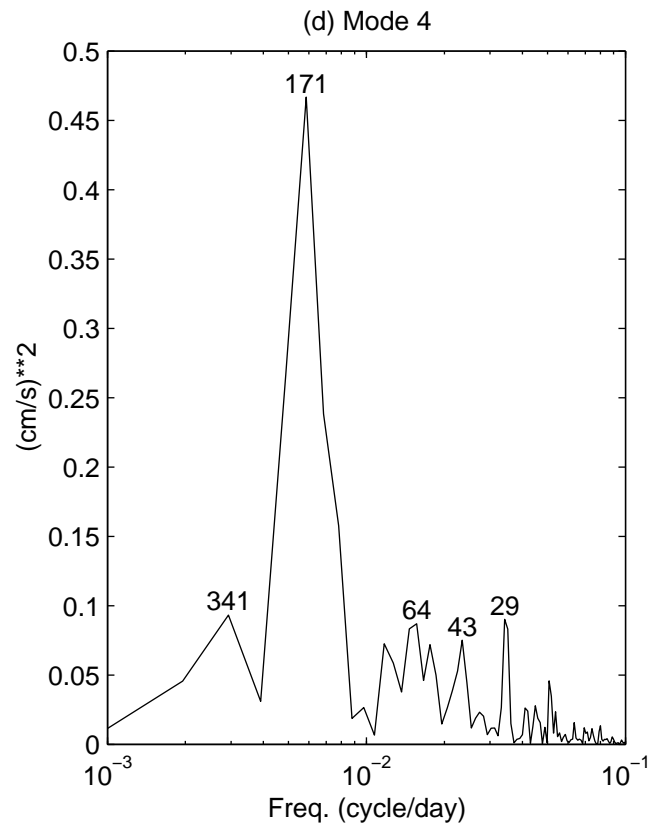
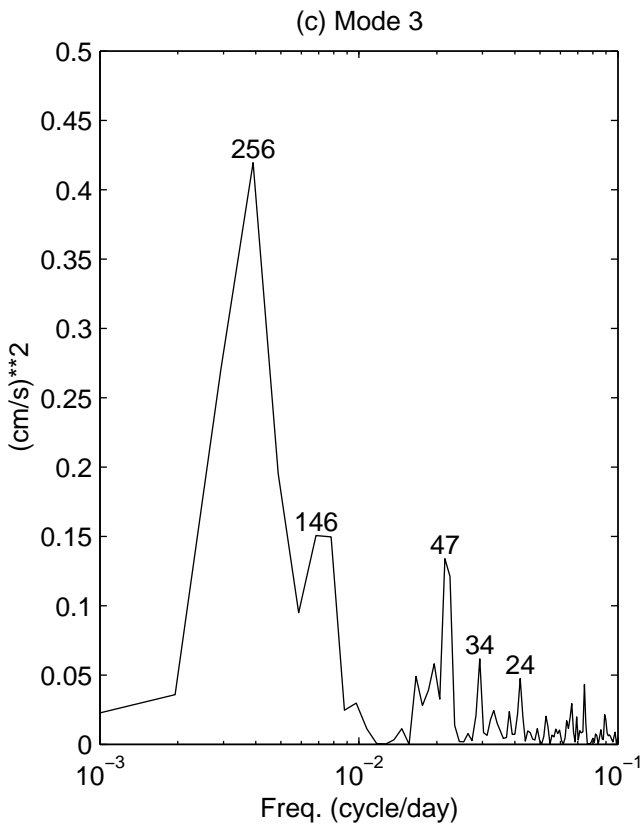
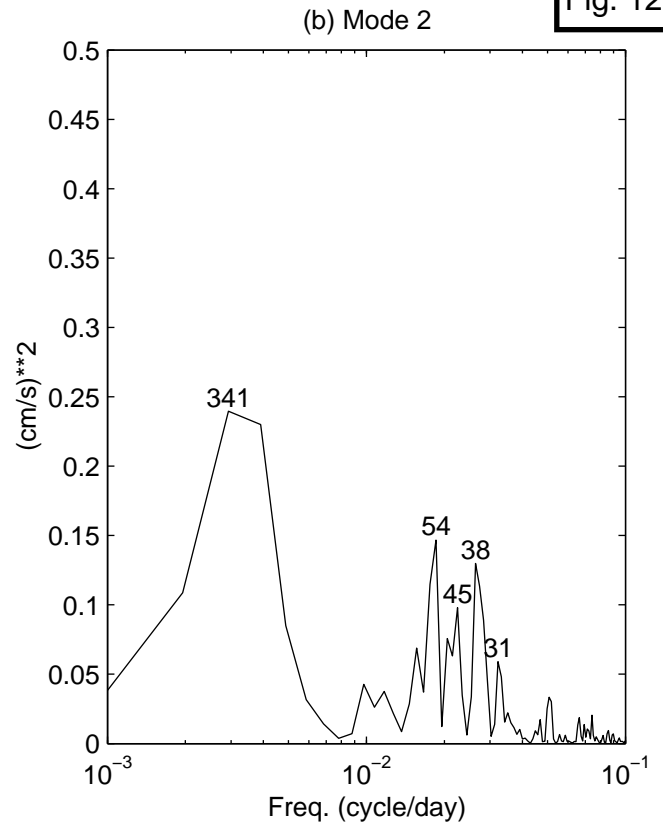
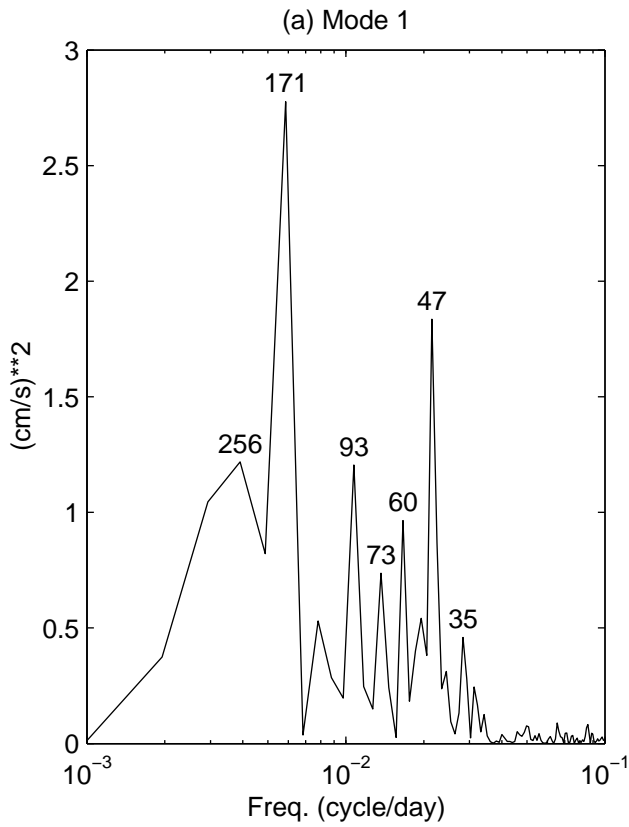


Fig. 13

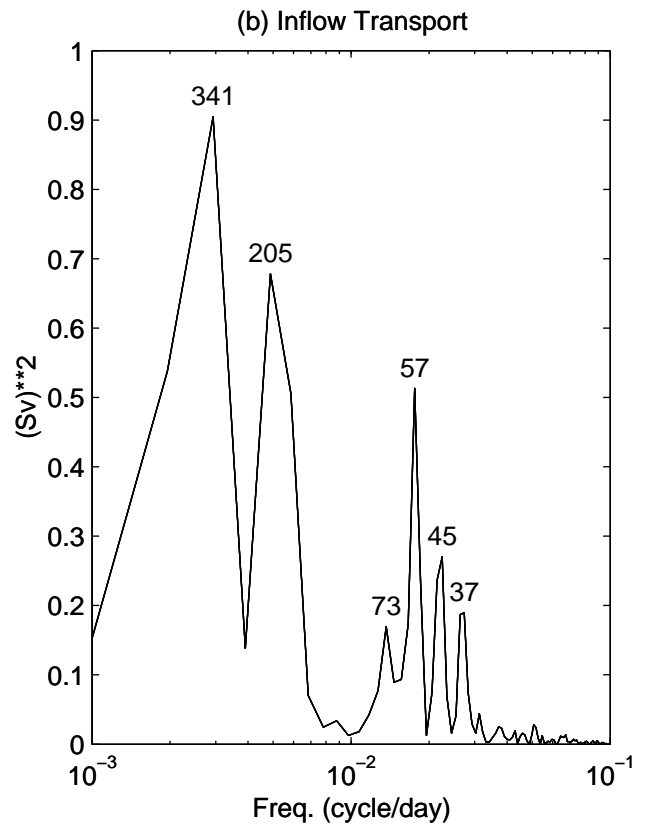
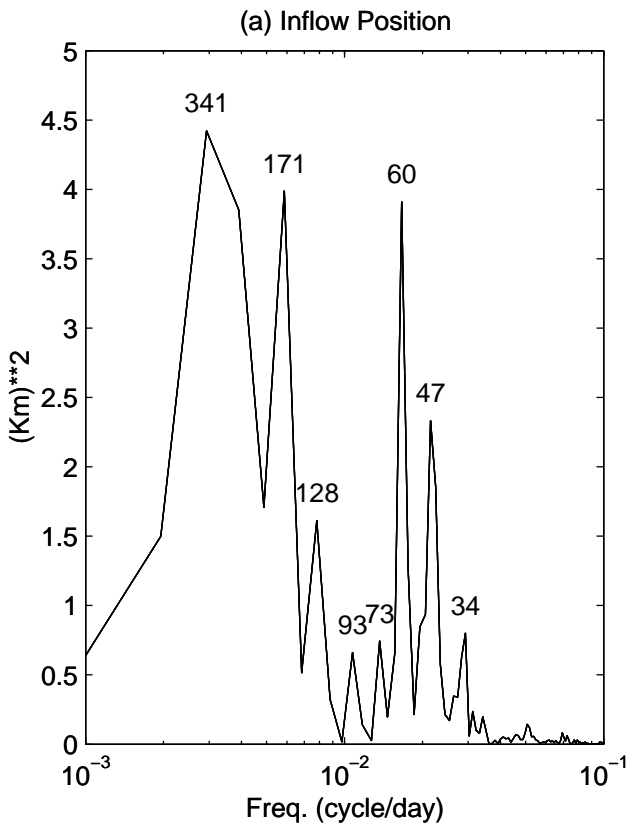


Fig. 14

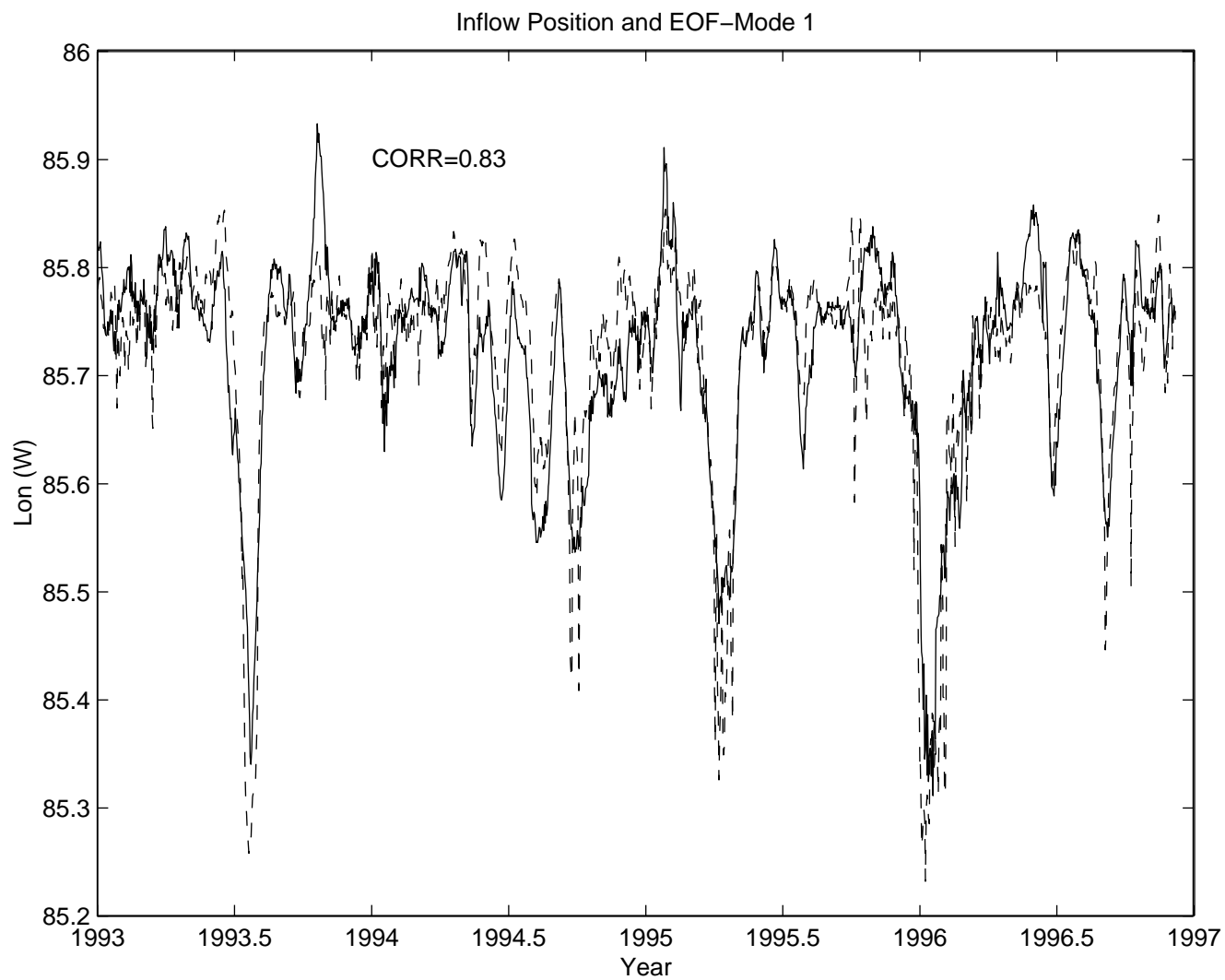


Fig. 15

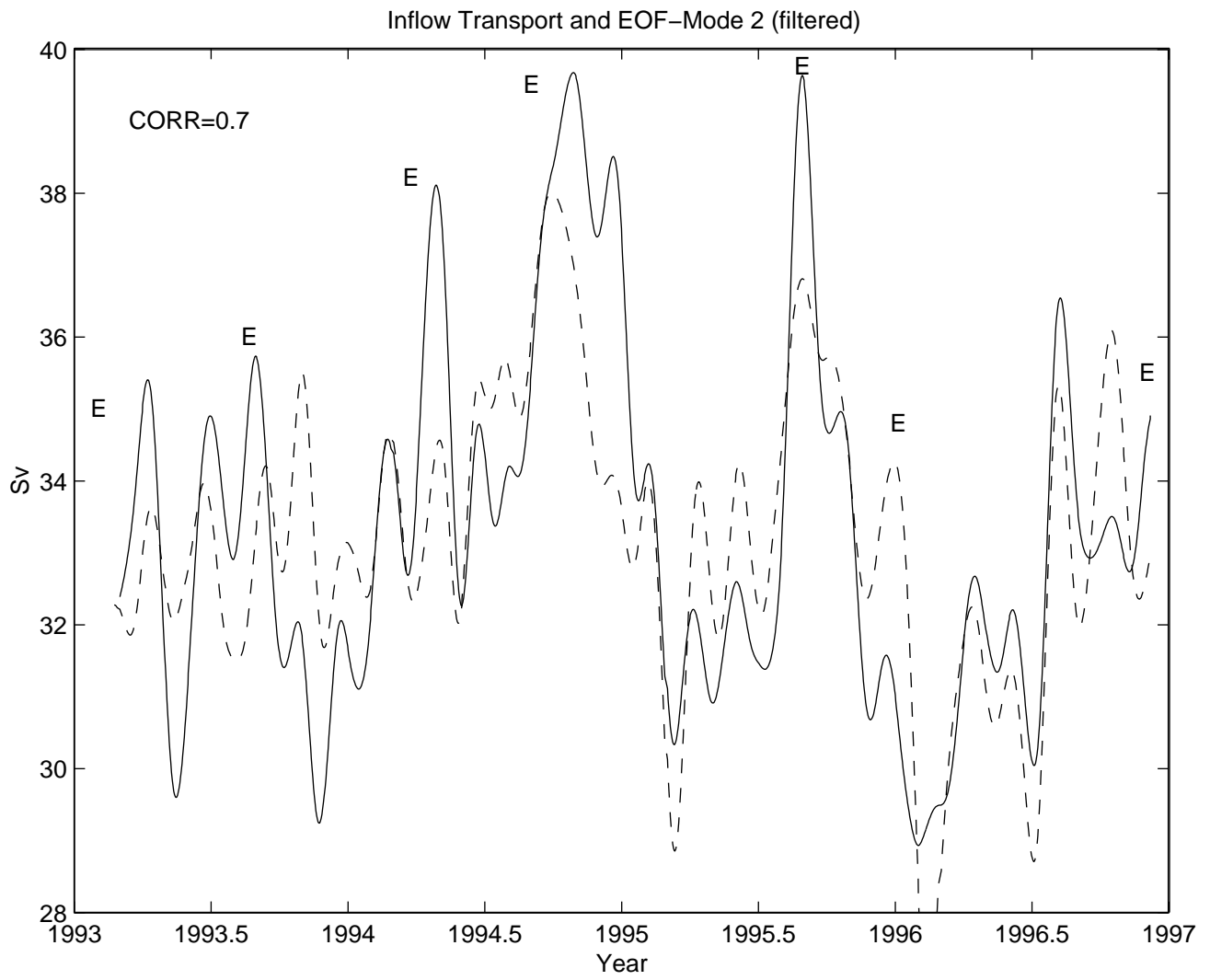


Fig. 16

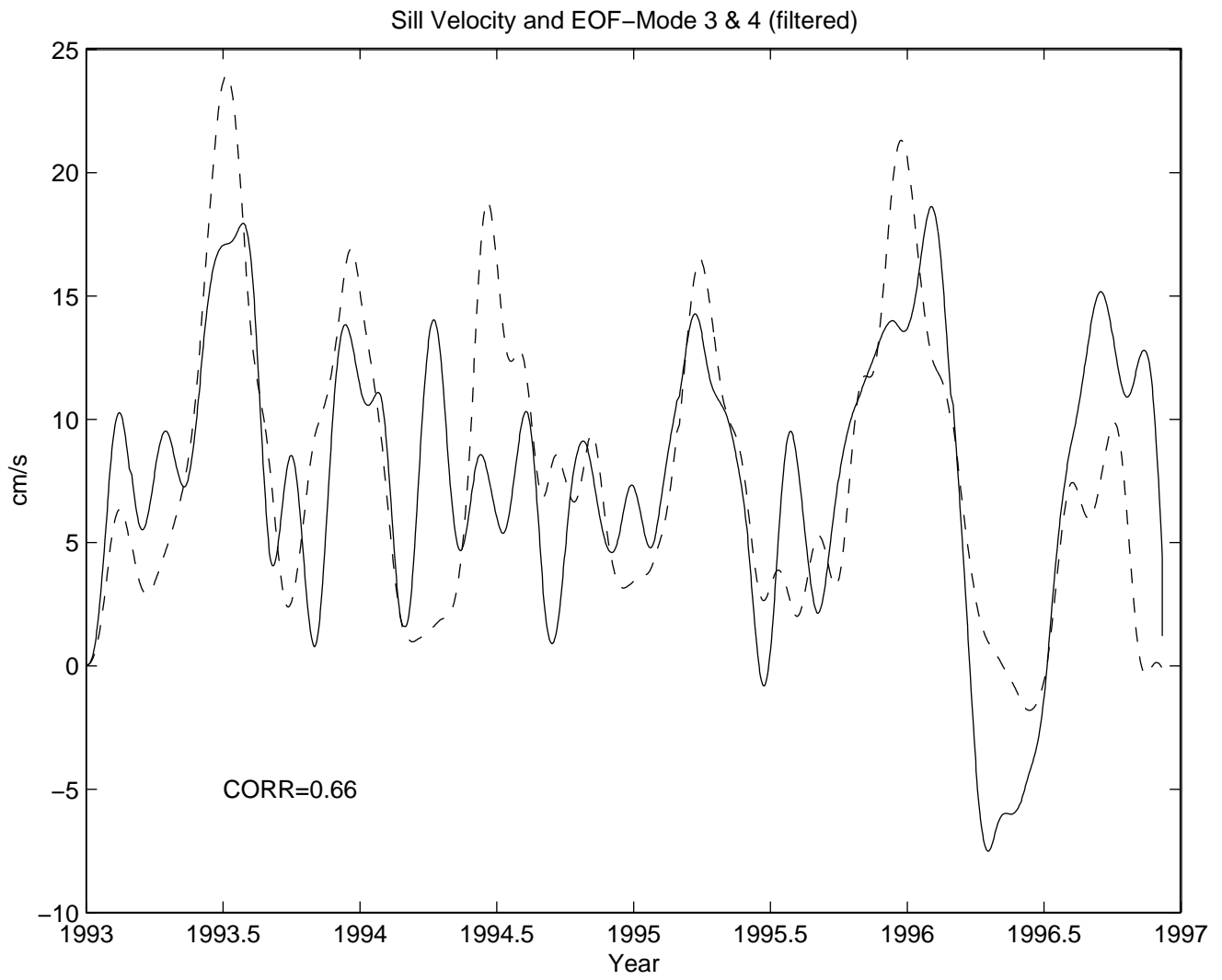


Fig. 17

